TRACE ELEMENT PARTITIONING BETWEEN TITANITE AND GROUNDMASS IN SILICIC VOLCANIC SYSTEMS

Michael Robert Ackerson

A thesis submitted to the faculty of the University of North Carolina at Chapel Hill in partial fulfillment of the requirements for the degree of Master of Science in the Department of Geological Sciences.

Chapel Hill
2011

Approved by:

Allen F. Glazner

Drew S. Coleman

Jonathan M. Lees

ABSTRACT

MICHAEL R. ACKERSON: Trace Element Partitioning Between Titanite and Groundmass in Silicic Volcanic Systems
(Under the direction of Dr. Allen F. Glazner)

Data for titanite and groundmass from seven Tertiary ignimbrites show a wide range of titanite trace-element concentrations and partitioning values. The range of partitioning values is due to lattice strain (with an ideal radius near Gd) and melt polymerization and is likely affected by the water content of the melt. The REEs, Y, Sc, Th and U are compatible in titanite whereas Rb, Sr, Ba and Pb are incompatible. Sector and growth zoning in titanite indicate disequilibrium crystal growth. Furthermore, differences in zoning, chemical composition and substitution mechanisms between volcanic and plutonic titanite suggest that volcanic titanite forms in systems characterized by down-T crystallization and high melt fractions whereas plutonic titanite forms at near-solidus conditions. Chemical similarities between titanite from the Fish Canyon magma system and plutonic titanite crystals provide evidence that the partitioning behavior of Fish Canyon titanite is the closest representation of titanite partitioning in plutonic systems.

ACKNOWLEDGEMENTS

I would like to acknowledge and thank my advisor Dr. Allen F. Glazner for his direction, scientific insight and guidance, which have been fundamental to the completion of this project and my growth as a scientist. I would also like to thank my committee member Dr. Drew Coleman for his support, perspective, comments and edits, and my committee member Dr. Jonathan Lees for his encouragement and assistance.

This project could not have been completed without the help of Drs. Alan Boudreau and Gary Dwyer of Duke University, Dr. Sohrab Habibi from the UNC Chemistry Department, and Drs. Jay Thomas and Dustin Trail at Rensselaer Polytechnic Institute. The editorial and technical aid of Ryan Mills, Kayla Ireland and Jesse Davis were crucial to making this a cohesive project, and the hours they have spent discussing petrology and geochemistry have helped broaden and enrich my scientific perspective. The endless emotional support of my family and Lara Gagrica has also been crucial. The Preston Jones and Mary Elizabeth Frances Dean Martin Trust Fund provided funding for this project.

TABLE OF CONTENTS

LIST OF TABLES……v

LIST OF FIGURES……..vi

LIST OF SYMBOLS……...vii

Chapter

I. INTRODUCTION……..1

Geologic Background……3

Geology of Samples…….10

II. METHODS……..16

III. RESULTS…….....19

Data Quality and Reproducibility of Results……...36

IV. DISCUSSION……41

Integrity of the Groundmass……41

Trace Element Partitioning……..44

Lattice Strain……46

Melt Polymerization…….48

Volcanic Versus Plutonic Titanite……...52

V. CONCLUSIONS……..…60

REFERENCES…….....62

LIST OF TABLES

Table

1. Sample locations and mineral assemblages……...11
2. Major-element compositions of volcanic groundmass……..14
3. Trace-element concentrations of titanite crystals……..21
4. Trace-element concentrations in volcanic groundmass…….26
5. Major-element compositions of selected titanite grains……29
6. Titanite/groundmass partitioning values for volcanic titanite crystals……..30
7. Results of Lattice Strain Modeling……49

LIST OF FIGURES

Figure

1. Structure and chemical substitutions in titanite……...4

2. Titanite stability in T-fO_2 space……...7

3. Sector zoning and coupled substitution in titanite……...9

4. Trace-element concentrations in volcanic titanite…….33

5. Trace-element concentrations in volcanic groundmass…….34

6. Titanite/groundmass trace-element partitioning values…….35

7. Monte Carlo simulation of Ce partitioning values in Fish Canyon Tuff……...39

8. Model of plagioclase contamination in Fish Canyon Tuff……43

9. Effect of melt composition and pressure on partitioning in experimental systems adapted from Green and Pearson (1985)……...45

10. Lattice strain modeling……..47

11. Effect of melt polymerization on partitioning values……...51

12. Sector and growth zoning in titanite from plutonic and volcanic rocks……...53

13. Rare earth element concentrations in plutonic and volcanic titanite……55

14. Al+Fe versus Ti in plutonic and volcanic titanite…….56

15. Eu/Eu* versus Yb concentrations in titanite from plutonic and volcanic rocks...58

LIST OF ABBREVIATIONS AND SYMBOLS

ASI	aluminum saturation index
C_g	concentration in groundmass
C_l	concentration in liquid
C_t	concentration in titanite
C_t/C_g	partitioning value
fO_2	oxygen fugacity
HFSE	high field strength element
ICP-MS	inductively coupled plasma mass spectrometer
LILE	large ion lithophile element
LSM	lattice strain model
m_t	mass of titanite
NBO/T	non-bridging oxygen/ tetrahedrally coordinated cation
REE	rare earth element
RSD	relative standard deviation
T	temperature
v_l	volume of liquid
ρ_l	density of liquid

I. INTRODUCTION

A primary goal of igneous petrology is to investigate the structural and chemical evolution of the continents. Fundamental to this goal is a need to understand how plutonic and volcanic rocks form, including the petrogenetic connections between them. Because mineral and melt trace-element compositions are sensitive to changes in temperature and pressure, they can yield information about the chemical and physical changes of a magma system that may not be reflected in the major element composition of the resultant rocks. In this way, trace-element analysis is a valuable tool that can provide insight toward understanding the processes that govern the formation of igneous rocks.

Accessory minerals provide insight into the trace-element composition of a rock and thereby help address questions about the formation of silicic plutonic and volcanic rocks and how they are related. Despite their low abundance, accessory minerals often contain a substantial portion of their host rock's trace element budget. Titanite ($(Ca,REE^{3+},Y)(Ti,Al,Fe^{3+})(O,F,OH)SiO_4$) is an example of such an accessory mineral. It contains high concentrations of trace elements including yttrium, the rare earth elements (REEs) and the high field strength elements (HFSEs; Henderson 1980, Green and Pearson 1986, Liferovich and Mitchell 2005, Marks et al. 2008). In many batholiths titanite, allanite and zircon may contain over 99% of the REEs (Gromet and Silver 1983). The presence of titanite significantly alters the trace element signatures of the melt phase and of the minerals that crystallize after titanite, thereby affecting a rock's overall trace element signature. This

makes it useful when determining the connection between plutonic and volcanic rocks (Glazner et al., 2008). In addition, titanite contains high enough concentrations of uranium to make it a useful mineral in geochronology (Zhang and Scharer 1996, Frost et al. 2000).

In order to accurately predict the effect of titanite crystallization on the composition of the melt and other phases, it is necessary to understand the degree to which titanite partitions trace elements in silicic systems and the factors affecting this partitioning. The trace-element content of titanite (and other minerals) is affected by factors that include lattice strain, melt polymerization and the water content of the melt. Partitioning values (defined as the ratio of an element's concentration in titanite compared to its concentration in the glass or groundmass) are a direct way to study the interaction between titanite and melt. Trace elements that fit most readily into a lattice site will impart the least amount of stress and strain on a crystal and will therefore be preferred in the crystal over more poorly fitting elements. This results in higher partitioning values for elements that have a better fit with the crystal lattice structure of titanite. Moreover, as the melt from which titanite is crystallizing becomes more polymerized, the compatibility of trace elements in the melt will change (Watson 1976, Watson 1977, Prowatke and Klemme 2005). Because the water content of a melt plays an important role in controlling melt polymerization, it too can affect trace-element partitioning into titanite.

Titanite is common in granodiorites (e.g. Glazner et al. 2008); however, it is impossible to determine partition coefficients for mineral phases in plutonic rocks because they do not contain a remnant melt phase. Unfortunately, titanite is rare in volcanic rocks (Nakada 1991), which has led to limited research into its crystallization and element partitioning. Developing a better understanding of the partitioning behavior of titanite

crystals in volcanic rocks therefore can provide an important first step into understanding the partitioning behavior of trace elements in plutonic rocks.

In this study, I explore the titanite/glass equilibrium in samples collected from Tertiary ignimbrites from the western United States and compare them with data for associated plutonic rocks and plutonic rocks of the Mesozoic Sierra Nevada batholith. The data suggest that partitioning values for volcanic titanite crystals are controlled by lattice strain and melt polymerization, and are likely affected by the water content of the melt. In addition, plutonic and volcanic titanite crystals exhibit distinct differences in their trace-element content, zoning and substitution mechanisms. This finding belies crystallization from similar systems and is consistent with the idea that most volcanic titanite forms through typical down-T crystallization of high melt-fraction systems whereas plutonic titanite forms at near- or sub-solidus conditions as is demonstrated for other phases in plutonic rocks.

Geologic Background

Titanite is an orthosilicate mineral whose structure allows for several significant substitutions. Its mineral structure consists of chains of Ti octahedra bounded by Si tetrahedra along with a sevenfold Ca site within the chains' (Fig. 1). Substitutions occur at the Ti and Ca sites, and at the underbonded O1 site that links the Ti octahedra, where F^- and OH^- can substitute for O^{2-}. The sevenfold Ca site is the location of REE, U, Th, Pb and other large ion lithophile element (LILE) substitutions. Substitution of Al^{3+}, Fe^{3+}, Nb^{3+} and the high field strength elements occurs in the octahedral Ti site .Whereas many substitution mechanisms have been proposed for titanite (Ribbe 1989, Frost et al. 2000, Vourinen and Helanius 2005), the conditions of crystallization dictate which mechanisms dominate. For example, in metamorphic rocks titanite can have up to 50% $CaAlSiO_5(OH)$ or $CaAlSiO_5F$

(Frost et al. 2000), whereas titanite with high concentrations of Na, Nb and Zr are reported from hydrothermal systems (Liferovich and Mitchell 2005).

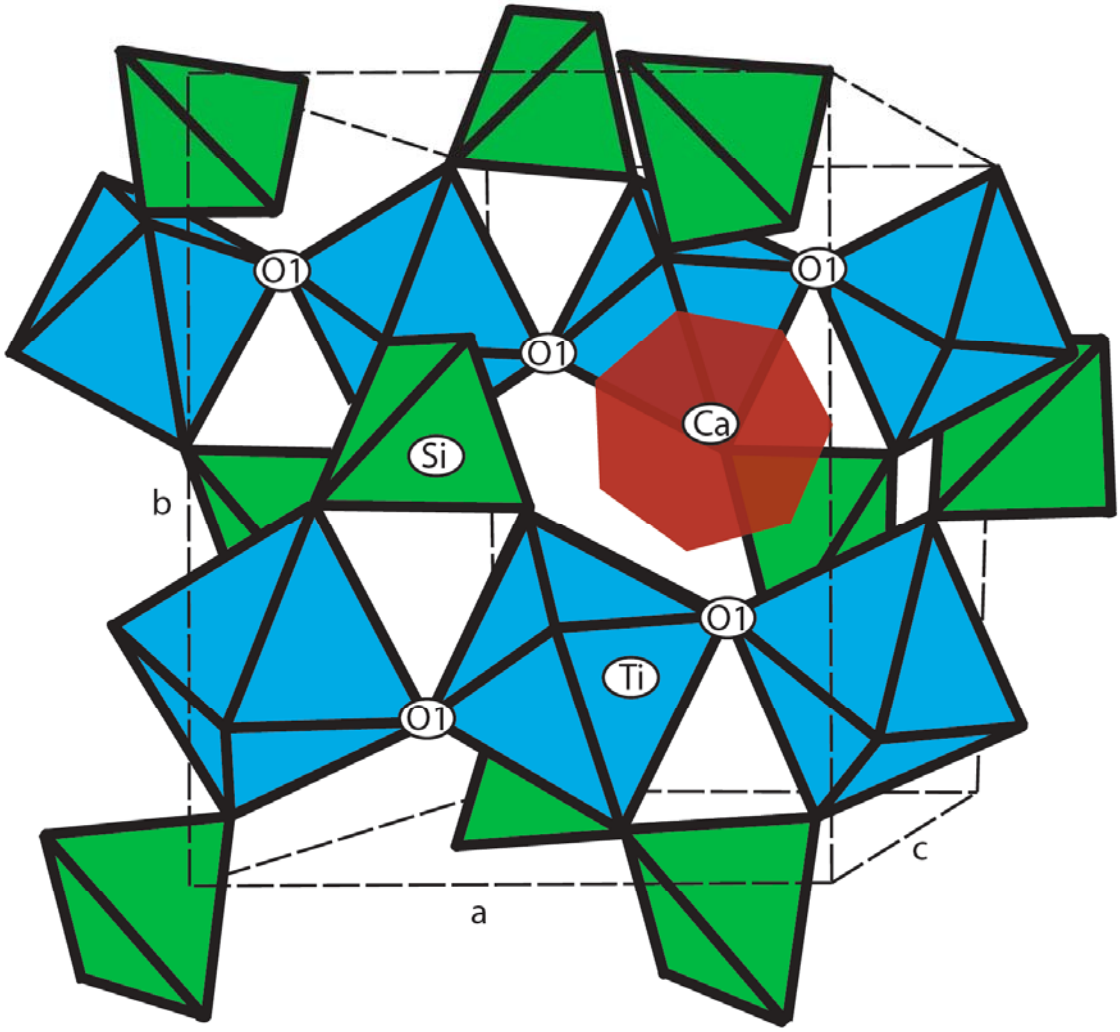

Figure 1: Structure and chemical substitutions in titanite. The primary trace-element substitutions that occur in titanite are the $REEs^{3+}$ and Y^{3+} into the seven-fold Ca^{2+} site and Al^{3+} and Fe^{3+} into the octahedral Ti^{4+} site. Substitution of OH^{-} and F^{-} can occur on the underbonded oxygen site (O1) between titanium octahedra (Ribbe 1980). Figure modified from Taylor and Brown, 1976.

In many igneous rocks, titanite crystals contain most of the REEs (Gromet and Silver 1983). Despite this, little work has been published on REE concentrations in titanite from silicic volcanic systems. Whereas determinations of trace element concentrations of titanite crystals in plutonic rocks are common (Simmons and Hedge 1978, Noyes et al. 1983, Broska et al. 2007), only a few studies have looked at volcanic titanite (Giannetti and Luhr 1983, Belkin et al. 1996, Della Ventura et al. 1999, Bachmann et al. 2005). Of partitioning studies in volcanic rocks, only one was performed using laser-ablation ICP-MS—the preferred modern method of trace-element data collection (Bachmann et al. 2005). Other studies collected data using electron microprobe analysis (Gianetti and Luhr 1983, Belkin et al. 1996).

The paucity of REE data for volcanic titanite is mirrored by the limited research on the conditions of titanite crystallization in magmatic systems. Titanite commonly occurs in intermediate to felsic igneous rocks, and a range of metamorphic conditions from low-pressure contact metamorphism of marls and limestones (Frost et al. 2000, Xirouchakis et al. 2001) to eclogite facies metamorphism of mafic igneous rocks (Oberti et al. 1991). In igneous rocks, the timing of the first appearance of titanite during crystallization is under debate. Bateman and Chappell (1979) used the euhedral crystal shape of titanite crystals in the Tuolumne Intrusive Suite of Yosemite National Park, California to infer early crystallization, whereas Nakada (1991) argued that the relative paucity of titanite in volcanic rocks favors late crystallization.

Even though little data exist on the crystallization conditions of titanite, high oxygen fugacity (fO_2) stabilizes titanite (Verhoogen 1962, Carmichael and Nicholls 1967, Lipman

1971, Whitney and Stormer 1985, Nakada 1991). The relationship between titanite stability and oxygen fugacity is displayed in figure 2, which shows the fO_2-T relations of titanite-bearing and titanite-absent dacitic and rhyolitic volcanic rocks from the western United States. Titanite-bearing rocks typically occur closer to the hematite-magnetite buffer curve, whereas titanite-absent rocks are found closer to the nickel-nickel oxide buffer curves. Wones (1989) attributes this to the reactions:

titanite + magnetite + quartz = hedenbergite + ilmenite + O_2 *(1)*

$3CaTiSiO_5 + 2Fe_3O_4 + 3SiO_2 = 3CaFeSi_2O_6 + 3FeTiO_3 + O_2$

where increasing oxidation favors the left side of the reaction.

Frost et al. (2000) deemed reaction (1) to be a function of oxygen fugacity, bulk chemistry and melt phase chemistry. They also considered the reaction:

titanite + annite = K-feldspar + ilmenite + quartz + CaO + H_2O *(2)*

$3CaTiSiO_5 + KFe_3AlSi_3O_{10}(OH)_2 = KAlSi_3O_8 + 3FeTiO_3 + 3SiO_2 + 3CaO_{(l)} + H_2O_{(l)}$

where CaO and H_2O are components of the melt phase.

Other intensive parameters can also affect titanite partitioning. Xirouchakis et al. (2001a,b) inferred a strong experimental correlation between T, fO_2, the activity of SiO_2 (a_{SiO2}), the assemblage of mafic mineral phases (ilmenite and magnetite) and titanite stability in quartz-saturated versus quartz-undersaturated mafic rocks. Green and Pearson (1985) demonstrated an experimental dependence on pressure of titanite REE partition coefficients. They showed that for titanite in silicic systems from 900˚ to 1120˚C and 7.5 to 30 kbar the

partition coefficients of REEs increase with increasing SiO_2 in the melt phase, decreasing temperature and increasing pressure.

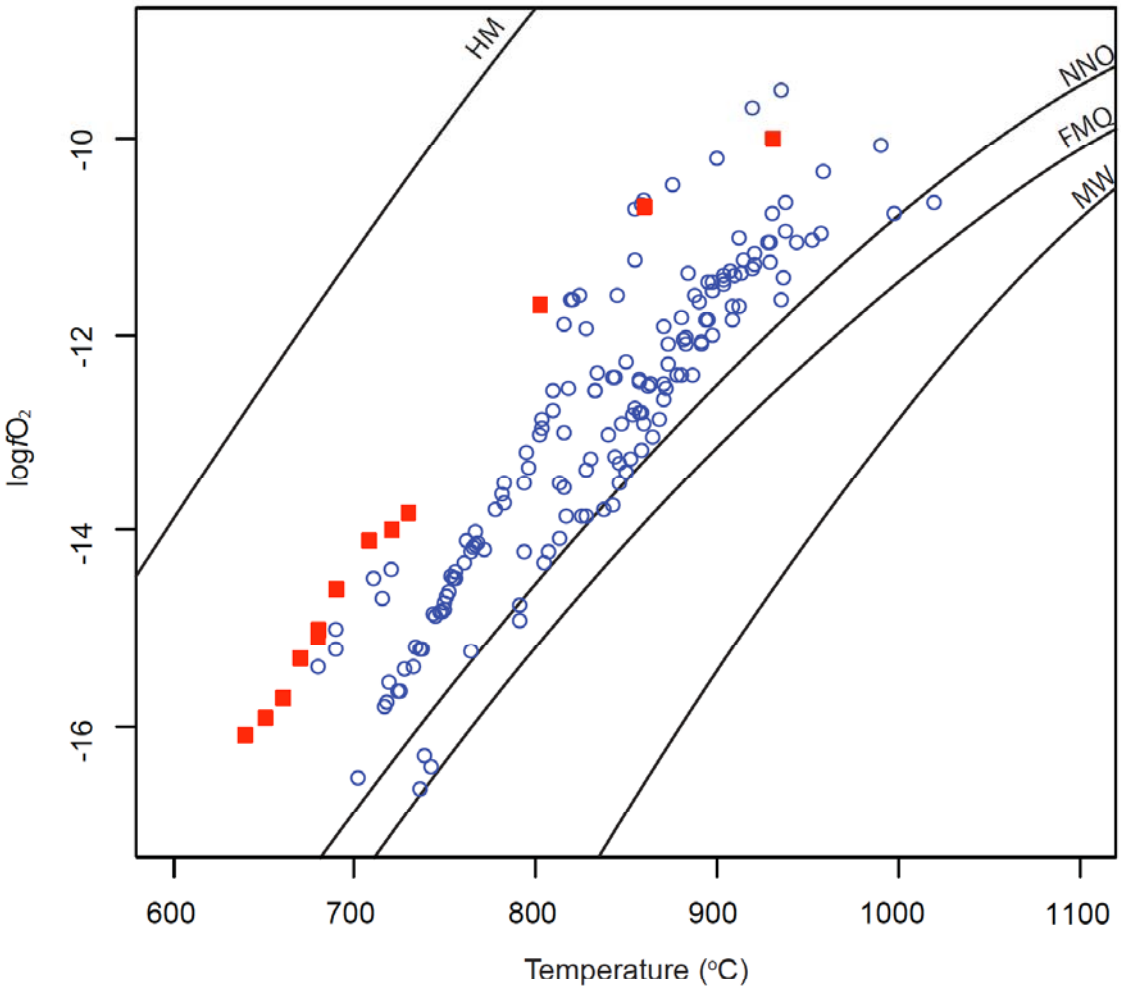

Figure 2: Plot of temperature versus the log of oxygen fugacity. Most values calculated using the two-oxide geothermometer of Andersen and Lindlsey (1988) with the solution model of Stormer (1983). Samples are dacites and rhyolites that do (red square (■)) and do not (blue circles (○)) contain titanite. Data collected are from Pallister et al. (2008), Venezky and Rutherford (1997), Whitney and Stormer (1985), Hildreth and Wilson (2007), Kratzmann et al. (2010), Browne et al. (2009), Lipman (1971), Maughan et al. (2002) , Carmichael (1991), and Luhr et al. (1984).

Titanite crystals in both volcanic and plutonic rocks typically exhibit sector-zoned cores (Fig. 3) with growth (oscillatory) zoned rims, demonstrating disequilibrium crystal growth (Paterson and Stephens 1992, Shore and Fowler 1996). The formation of sector zoning is aided by factors including rapid crystal growth and anisotpopic incorporation of trace elements along the crystals surface (Watson and Liang, 1995). In igneous titanite, crystal growth is predominantly along the {111} crystal faces. When crystal growth is rapid, slow-growing faces dominate the crystal morphology. Coupled with differences in crystal face growth rates is the anisotropic preference for the REEs and Y to occur along the {100} sectors, whereas Al and Fe occur preferentially along the {111} sectors (Paterson and Stephens, 1992).

Because disequilibrium zoning in igneous titanite is commonplace (Paterson and Stephens 1992, Vuorinen and Halenius 2005, McLeod et al. 2011), mineral/groundmass partitioning values cannot be considered equilibrium partition coefficients. Disequilibrium partitioning values should be used with reserve when being applied to equilibrium fractionation models. The interpretation of zoning patterns in minerals (in particular oscillatory zoning) is dependent upon their formational environment. Elements with partitioning values greater than one (meaning the element is compatible in the mineral phase over the melt phase) that crystallize from silicic volcanic systems can have oscillatory zoning caused by crystal growth occurring more rapidly than the rate at which trace elements are transported to the crystal-melt interface (Paterson and Stephens, 1991). Crystals forming in near-solidus systems where thermal cycling is likely (such as the K-spar megacryst formation

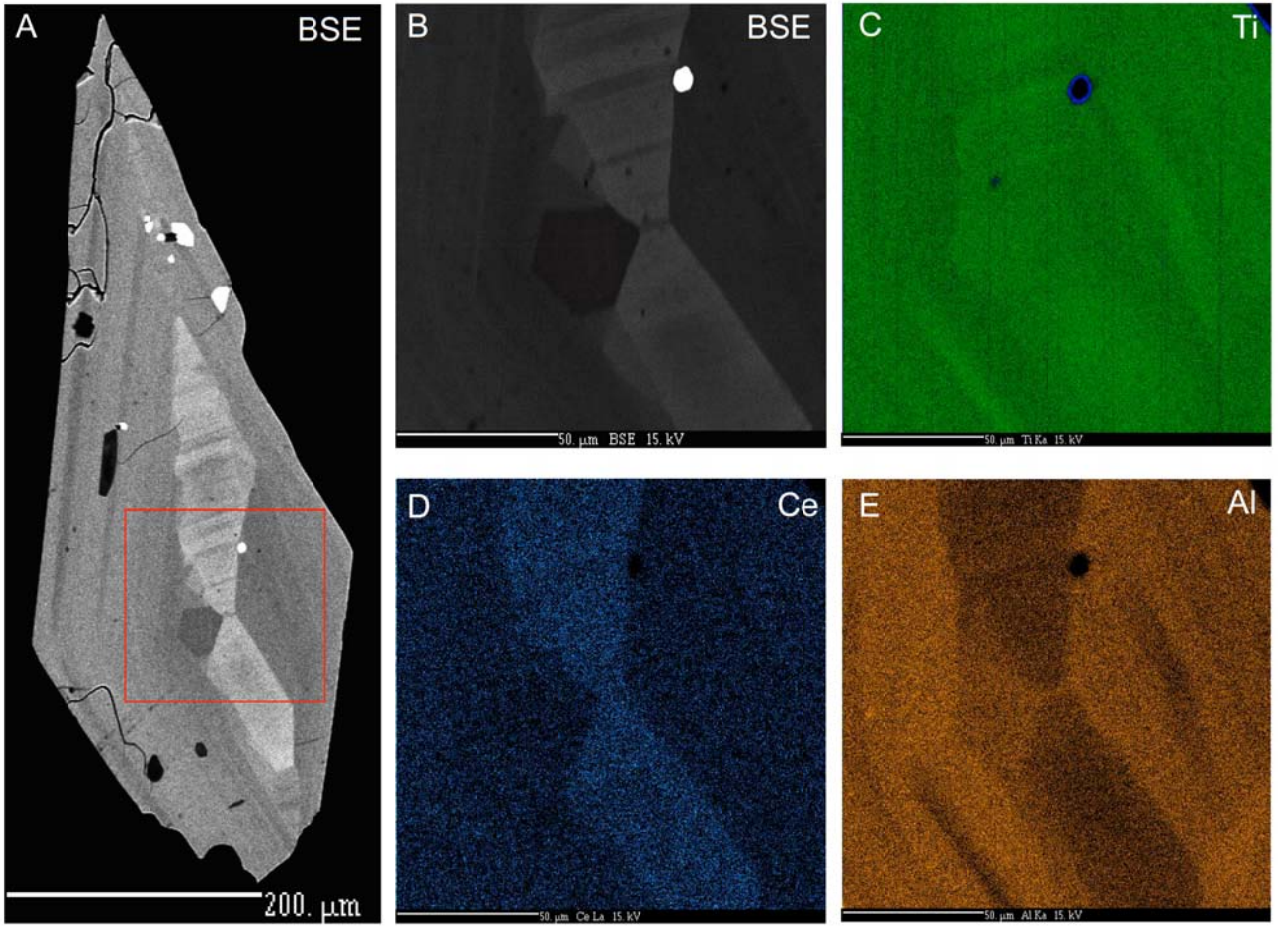

Figure 3: Sector zoning and coupled substitution in titanite from the Ammonia Tanks Member. (A,B) BSE image of titanite showing crystal morphology defined by the {111} indices, with growth along {100} visible as sectors in the center of the grain. (C,D,E) Titanium, cerium and aluminum composition maps of zoning with a positive correlation between brightness and concentration. Preferential substitution of the REEs along {100} is demonstrated by the brightness of Ce on the {100} planes relative to {111}. Conversely, Al+Fe preferentially substitute onto the {111} faces. Furthermore, the charge-balanced substitution of Al+Fe for Ti is shown by the inverse relation between Ti and Al brightness in (C) and (E).

discussed by Johnson and Glazner, 2010) will exhibit oscillatory zoning that is a consequence of thermally induced periods of melt creation and subsequent crystal growth.

Geology of Samples

Volcanic and plutonic samples collected for this study (Table 1) are part of the silicic ignimbrite flare-up that occurred in the western United States during the Cenozoic Era and range in age from Eocene to Miocene (36.7-11.3 Ma). Additionally, data are presented for plutonic rocks of the Mesozoic Sierra Nevada batholith (Gaschnig 2005, Davis et al. 2011). Volcanic rocks sampled range in composition from dacite to rhyolite and vary widely in crystallinity, temperature and water content. Plutonic rocks are quartz monzonites and granodiorites.

Two samples were analyzed from the Timber Mountain-Oasis Valley Caldera complex of southwestern Nevada—a pumice sample from the Ammonia Tanks Member of the Timber Mountain caldera and a whole-rock sample from the Tiva Canyon Member of the Oasis Valley caldera. Both units are rhyolitic ash-flow tuffs. The tuffs existed as relatively dry magmas (1-2 wt% H_2O) and formed at temperatures ranging from 816 °C for the Ammonia Tanks to 838 °C for Tiva Canyon (Lipman 1966, Byers et al. 1976, Christiansen et al. 1977, Broxton et al. 1989, Mills et al. 1997, Bindeman et al. 2006).

The Fish Canyon Tuff and Pagosa Peak dacite from the La Garita caldera system in the San Juan volcanic field of Colorado were also analyzed. The Fish Canyon magma system is thought to be a reactivated plutonic system that erupted nearly homogeneous crystal-rich dacitic magma in three stages. The Pagosa Peak dacite is a precursor to the main unit erupted from the caldera, the Fish Canyon Tuff. The Fish Canyon magma system existed at temperatures near 760 °C and contained 5 wt% H_2O (Johnson and Rutherford 1989, Lipman

Table 1: Sample locations and mineral assemblages

Unit	Location	Rock Type	Mineral Assemblage†
Ammonia Tanks Member*	N36°59'50" W116°33'39"	Rhyolite	Ap, Bt, Cpx, Hbl, Il, Kfs Mag, Pl, Qtz, Ttn, Zrn
Tiva Canyon Member*	N36°53'48" W116°27'30"	Rhyolite	Ap, Bt, Hbl, Il, Kfs Mag, Pl, Qtz, Ttn, Zrn
Pagosa Peak Dacite	N37°32'34.5" W106°47'53.2"	Dacite	Ap, Bt, Hbl, Il, Kfs, Mag Pl, Po, Qtz, Ttn, Zrn
Fish Canyon Tuff	N37°36'43.0" W106°42'13.2"	Dacite	Ap, Bt, Hbl, Il, Kfs, Mag Pl, Po, Qtz, Ttn, Zrn
Bonanza Rhyolite	N38°09'16.2" W106°16'28.9"	Rhyolite	Bt, Hbl, Kfs, Mag, Pl Qtz, Ttn, Zrn
Peach Springs Tuff	N34°47'20.4" W116°19'05.9"	Rhyolite	Bt, Hbl, Il, Kfs, Mag Pl, Qtz, Ttn, Zrn
Wall Mountain Tuff	N38°50'32.8" W105°59'00.4"	Rhyolite	Ap, Bt, Hbl, Il, Kfs Mag, Pl, Qtz, Ttn, Zrn

*Samples collected by Frost (1987), donated to project from the scientific collections at Michigan State University by Dr. Thomas Vogel.
†Mineral abbreviations from Kretz (1983): Ap=apatite, Bt=biotite, Cpx=clinopyroxene, Hbl=hornblende, Il=ilmenite, Kfs=K-feldspar, Mag=magnetite, Pl=plagioclase, Po=pyrrhotite, Qtz=quartz, Ttn=titanite, Zrn=zircon

et al. 1997, Bachmann et al. 2002, Bachmann et al 2008, Lipman and McIntosh 2008). The Fish Canyon Tuff sample was collected from the type locality of the Ar-Ar sanidine standard FCs (Renne et al. 1998).

Three other samples were analyzed from the San Juan volcanic field. These include volcanic samples from the phenocryst-poor rhyolitic Bonanza Tuff (Varga and Smith 1984, Lipman and McIntosh 2008) and the low-silica rhyolite Wall Mountain Tuff (Chapin and Lowell 1979, McIntosh and Chapin 2004) and a plutonic sample from a quartz monzonite of the Mount Princeton Batholith (Lipman 2007, Lipman and McIntosh 2008).

A final volcanic sample was analyzed from the high-K rhyolite Peach Springs Tuff of California (Glazner et al. 1986, Glazner 1988, Pamukcu 2010). Although the titanite grains in this sample were euhedral and unaltered, much of the groundmass was altered to either zeolite or clay (likely montmorillonite). This alteration is evident in the major-element analyses of the Peach Springs Tuff "groundmass" (Table 2). Because the REEs are relatively immobile in groundmass during alteration (Zielinski 1982), they may not have moved when the groundmass was altered, and the REE analyses may be more or less the same as the initial groundmass concentration. Still, the partitioning values determined for the Peach Springs Tuff may not accurately represent the partitioning behavior between titanite crystals and melt.

To study the differences between plutonic and volcanic titanite crystals, samples were also analyzed from the Sierra Nevada Batholith. Two samples were analyzed from the John Muir Intrusive Suite of the Sierra Nevada Batholith–a sample of the Lake Edison Granodiorite (SNBa-1, SNBa-2) and a sample of the modally-layered Round Valley Peak Granodiorite (SNBb). SNBa titanite crystals came from sample Kle07-05 collected by Davis

(2010). SNBb titanite crystals came from sample Rvp-2 collected by Gaschnig (2005) (Bateman 1992, Gaschnig 2005, Davis et al. 2011). Foley (2010) showed that layered granodiorite from this unit is locally exceptionally rich in titanite.

Table 2: Major-element compositions of volcanic groundmass*

	Ammonia Tanks			Tiva Canyon			Pagosa Peak Dacite		
	Wt. %	SD	RSD	Wt. %	SD	RSD	Wt. %	SD	RSD
SiO_2	75.5	0.78	1.0	72.21	0.76	1.1	74.87	0.78	1.0
TiO_2	0.11	0.06	54.5	0.17	0.06	35.3	0.1	0.06	60.0
Al_2O_3	12.3	0.22	1.8	13.16	0.22	1.7	12.45	0.22	1.8
FeO	0.25	0.18	72.0	0.42	0.18	42.9	0.22	0.18	81.8
MnO	0.01	-	-	0.01	-	-	0.01	-	-
MgO	0.02	0.04	200.0	0.08	0.16	200.0	0.07	0.12	171.4
CaO	0.24	0.06	25.0	0.56	0.06	10.7	0.44	0.06	13.6
Na_2O	3.62	0.1	2.8	2.94	0.1	3.4	2.95	0.1	3.4
K_2O	4.94	0.14	2.8	5.61	0.14	2.5	4.45	0.12	2.7
Total	97			95.15			95.53		
ASI	1.05			1.08			1.19		
NBO/T	0.15			0.16			0.13		

	Fish Canyon Tuff			Bonanza Rhyolite			Peach Springs Tuff		
	Wt. %	SD	RSD	Wt. %	SD	RSD	Wt. %	SD	RSD
SiO_2	75.05	0.78	1.0	76.02	0.8	1.1	61.32	0.64	1.0
TiO_2	0.14	0.06	42.9	0.09	0.06	66.7	0.12	0.06	50.0
Al_2O_3	12.99	0.22	1.7	12.02	0.22	1.8	15.55	0.26	1.7
FeO	0.17	0.16	94.1	0.39	0.18	46.2	0.65	0.2	30.8
MnO	0	-	-	0	-	-	0	-	-
MgO	0.09	0.12	133.3	0.09	0.16	177.8	4.17	0.24	5.8
CaO	0.89	0.06	6.7	0.45	0.06	13.3	1.14	0.06	5.3
Na_2O	3.35	0.1	3.0	3.18	0.1	3.1	0.14	0.06	42.9
K_2O	4.75	0.14	2.9	5.38	0.14	2.6	0.16	0.1	62.5
Total	97.44			97.63			83.25		
ASI	1.05			1.01			2.45		
NBO/T	0.15			0.16			0.09		

* Standard deviation (2σ) is in ppm. RSD is reported in %.

Table 2 (cont'd): Major-element compositions of volcanic groundmass*

	Wall Mountain Tuff		
	Wt. %	SD	RSD
SiO_2	73.53	0.76	1.0
TiO_2	0.27	0.06	22.2
Al_2O_3	14.75	0.22	1.5
FeO	0.32	0.18	56.3
MnO	0.01	-	-
MgO	0.1	0.18	180.0
CaO	0.47	0.06	12.8
Na_2O	3.71	0.1	2.7
K_2O	6.05	0.14	2.3
Total	99.2		
ASI	1.09		
NBO/T	0.17		

* Standard deviation (2σ) is in ppm. RSD is reported in %.

II. METHODS

Titanite crystals and groundmass were separated from bulk rock samples using standard techniques including steel-plate disc milling, water tabling, methylene iodide density separation and magnetic separation. Once separated from the other phases, titanite crystals were selected for analysis on the basis of euhedral crystal shape and lack of inclusions (to reduce trace-element contamination). Primary crystal and groundmass selection was performed using a non-polarized binocular microscope. Selected crystals and groundmass were scrutinized under cross-polarized light to identify any inclusions that may have been missed in ordinary light.

Inclusion-free titanite and groundmass samples were weighed and prepared for solution ICP-MS analysis. Titanite crystals were separated into replicate groups (6-18 crystals/replicate) and weighed using a Sartorius 4504 MP8 Ultra Micro balance with an accuracy of ± 0.2 μg. Because volcanic groundmass can contain up to 300 times lower REE concentrations than titanite crystals (Bachmann et al. 2005), the mass of groundmass analyzed was approximately 250-300 times greater than the mass of titanite analyzed. Once weighed, the crystal and groundmass replicate groups were placed individually in 4:1 mixtures of concentrated HF and HNO_3 in a tightly sealed Teflon beaker and dissolved on a 130°C hot plate for five days. After this interval, the beakers were placed in an ultrasonic cleaner for 30-90 minutes. The solutions were dried and re-dissolved in 5% HNO_3 for analysis.

Once dissolved in HNO_3, titanite and groundmass trace-element compositions were analyzed using solution ICP-MS on a Varian 820 ICP-MS. Calibration curves were created using the Claritas PPT multi-element standard solutions CLMS-1 and CLMS-2 from SPEX CertiPrep. Analyte concentrations were recorded as concentrations (ppb) in the analyzed solution. Concentrations in titanite were calculated using:

$$C_t = C_l \times \frac{v_l \rho_l}{m_t} \qquad (1)$$

where C_t is the concentration in titanite (ppm), C_l is the concentration in the liquid analyte in ppm, and m_t and v_l are the masses of the titanite crystals and the volume of the liquid, respectively. ρ_l is the density of the liquid, which is assumed to be 1 g/cm^3.

Accurate solution ICP-MS analysis requires a constant flow of solution through the nebulizer into the analyzer. The nebulizer creates an aerosol out of the analyte solution to aid in ionizing the solution when it reaches the plasma. The opening of the nebulizer is small and can easily be clogged by particulate matter, impeding the flow of sample to the machine. Before running titanite and groundmass solutions through the ICP-MS, they were filtered to remove any particulates that could clog the nebulizer and impede flow into the ICP-MS. Flow of solution into the ICP-MS is monitored using ^{115}In ratios. An internal standard of known ^{115}In concentration is continuously pumped into the ICP-MS system while analyzing samples, blanks, and standards. The ^{115}In ratio is a ratio of the ^{115}In of the sample to the ^{115}In of the blank. The count intensity of a sample is divided by the ^{115}In ratio as a way to correct for changes in flow.

The major-element compositions of titanite and groundmass were analyzed using electron probe micro-analyzers. Titanite crystals were analyzed using the Cameca SX-100 at Rensselaer Polytechnic Institute, with a LaB_6 electron beam. Data reduction and ZAF

corrections were performed using SX logger software. The beam was run at 15 keV and 20 nA, with a spot size of 10 μm. Elements were standardized to a suite of silicate mineral standards. Groundmass samples were analyzed using a Cameca Camebax electron probe micro-analyzer (EPMA) at Duke University. Data correction was performed using ZAF correction in the Cameca PAP software. The beam spot size was typically 10-15 μm, with an accelerating voltage of 15 keV and a beam current of 15 nA. Volcanic groundmass was standardized using the 1921 Kilauea basalt and Cam 112 obsidian standards.

III. RESULTS

Trace-element concentrations in plutonic and volcanic titanite crystals are in good agreement with laser ablation ICP-MS analyses of plutonic titanite (Marks et al., 2008) and volcanic titanite from the Fish Canyon Tuff and Pagosa Peak dacite (Bachmann et al., 2005). Overall, concentrations of individual elements range over an order of magnitude between samples (Table 3, Fig. 4). Titanite crystals of the Fish Canyon Tuff and Pagosa Peak dacite contain the lowest REE concentrations of the volcanic samples and are similar in trace-element composition to the plutonic titanite crystals. REE concentrations in the Bonanza Rhyolite and Ammonia Tanks Member are greater than concentrations previously reported for any titanite. All titanite samples exhibit Eu anomalies.

Groundmass trace-element concentrations are highly variable, but also significantly lower than titanite concentrations (Table 4, Fig. 5). The Ammonia Tanks Member and Peach Springs Tuff have the lowest trace-element concentrations, whereas the Wall Mountain Tuff and Tiva Canyon Member have the highest concentrations. Groundmass Eu anomalies are all negative except for a small positive anomaly in Fish Canyon Tuff groundmass.

Major-element analyses of titanite crystals show that SiO_2 content between samples remain relatively constant at around 29 wt% whereas most other major elements vary noticeably between samples (Table 5). Totals are lower than 100% (ranging from 93.26-97.54%) because only one REE was measured (Ce_2O_3). With the exception of the altered Peach Springs Tuff, major-element analyses of volcanic groundmasses are typically high in

silica (around 75 wt% SiO_2). Major-element analyses of the groundmass yields totals averaging above 95%.

Despite varying over an order of magnitude, trace-element partitioning values between titanite crystals and groundmass of the seven volcanic units display similar shapes (Fig. 6). Although there is a general decrease in the REE content of titanite crystals from light (LREE) to heavy (HREE) (Fig. 4), partitioning values display a curve peaking near the middle (MREE), with the HREEs being slightly more enriched than the LREEs. Yttrium partitioning values (Table 6) are higher than the REE partitioning values and are closest to the light-middle REEs. Partitioning values for the REEs are lowest for the Wall Mountain Tuff, whereas the Peach Springs Tuff and Ammonia Tanks Member have the highest partitioning values. Partitioning values for Ba and Sr— which substitute into the Ca-site in titanite— fluctuate around 1. Whereas Sc Th and U are consistently compatible in titanite, Rb and Pb are typically incompatible.

Table 3: Trace-element concentrations of titanite crystals.*

	Ammonia Tanks Member			Tiva Canyon Member			Pagosa Peak Dacite		
Element	C_t	SD	RSD	C_t	SD	RSD	C_t	SD	RSD
Sc	76.7	8.3	11	92	20	22	44	15	33
Rb	47.6	4.4	9.2	37	15	40	13	4.1	32
Sr	8.4	4.0	47	72	70	97	83	20	24
Y	18400	2700	15	13300	1900	14	7100	1900	27
Ba	62	87	140	156	91	58	104	66	64
La	2070	350	17	2290	330	15	2940	620	21
Ce	9000	1400	15	9500	1400	15	9800	2200	23
Pr	1520	220	14	1730	340	20	1400	340	24
Nd	6520	840	13	8300	1600	20	5500	1300	24
Sm	1910	260	14	2160	480	22	1010	260	26
Eu	45.6	9.4	21	267	72	27	155	31	20
Gd	1770	240	14	1870	400	21	910	230	25
Tb	681	88	13	630	130	20	272	73	27
Dy	1880	250	13	1540	310	20	650	180	28
Ho	343	46	13	265	49	19	123	34	28
Er	920	130	14	680	110	16	374	97	26
Tm	110	16	15	73.8	8.9	12	48	13	26
Yb	585	89	15	383	44	11	305	79	26
Lu	63	9.8	16	41.4	5.1	12	39.5	9.8	25
Pb	9.2	2.0	22	12.1	9.8	81	6.6	2	30
Th	233	29	12	153	12	7.8	280	54	19
U	39.1	3.8	9.7	28.2	1.9	6.7	101	21	20

*Concentrations and standard deviation (2σ) are in ppm. RSD is reported in %.

Table 3 (cont'd): Trace-element concentrations of titanite crystals.*

	Fish Canyon Tuff			Bonanza Rhyolite			Peach Springs Tuff		
Element	C_t	SD	RSD	C_t	SD	RSD	C_t	SD	RSD
Sc	36.7	3.1	8.5	117.25	0.62	0.53	103	37	36
Rb	6.3	2.2	34	7.5	9.1	120	4.1	1	25
Sr	83.7	8	9.5	16.6	5.8	35	28	19	68
Y	6410	680	11	13070	490	3.8	11300	3800	34
Ba	65	14	22	86.1	9.4	11	45	13	29
La	2790	240	8.7	3593	30	0.84	3000	1200	41
Ce	9160	710	7.7	13740	180	1.3	11600	4600	40
Pr	1280	91	7.1	2083	78	3.7	1830	690	38
Nd	5060	450	8.9	8150	390	4.8	7600	2600	34
Sm	941	89	9.4	1660	100	6.9	1700	540	32
Eu	156	13	8	61	2.8	4.7	128	47	37
Gd	853	82	9.6	1504	62	4.1	1500	470	32
Tb	251	26	10	496	22	4.5	1480	140	30
Dy	595	67	11	1273	78	6.1	1170	340	29
Ho	111	12	11	236	11	4.7	211	69	33
Er	338	35	10	664	21	3.1	580	200	34
Tm	43.6	4.4	10	78.1	2.8	3.5	66	23	35
Yb	277	25	8.9	429	9.8	2.3	350	130	36
Lu	36.1	3.2	8.9	48.07	0.34	0.63	40	15	38
Pb	4.82	0.29	6.1	8.55	0.97	11	6.6	2.7	41
Th	278	22	7.8	429	23	5.3	240	100	45
U	103.3	7.4	7.2	98.9	5.2	5.3	35	15	43

*Concentrations and standard deviation (2σ) are in ppm. RSD is reported in %.

Table 3 (cont'd): Trace-element concentrations of titanite crystals.*

	Wall Mountain Tuff†		
Element	C_t	SD	RSD
Sc	121	27	22
Rb	3.5	1.9	52
Sr	70	39	56
Y	8300	1700	21
Ba	77	50	65
La	2070	430	21
Ce	8100	1700	20
Pr	1400	300	21
Nd	6600	1400	21
Sm	1460	320	22
Eu	181	43	24
Gd	1230	260	21
Tb	380	80	21
Dy	890	190	21
Ho	159	34	22
Er	437	90	21
Tm	50	10	20
Yb	284	56	20
Lu	35.2	7.1	20
Pb	35	13	38
Th	264	51	19
U	124	23	18

*Concentrations and standard deviation (2σ) are in ppm. RSD is reported in %.
† error reported for Wall Mountain Tuff crystals is calculated from the average relative standard deviation of the other six titanite samples

Table 3 (cont'd): Trace-element concentrations of titanite crystals.*

	Lake Edison Granodiorite			Lake Edison Granodiorite			Round Valley Peak Granodiorite		
Element	C_t	SD	RSD	C_t	SD	RSD	C_t	SD	RSD
Sc	6.9	0.44	6.4	7.92	0.31	3.9	22.1	5	23
Rb	-	-	-	-	-	-	2.8	2	73
Sr	-	-	-	-	-	-	107	18	16
Y	1408	29	2.1	1390	360	26	3960	140	3.6
Ba	-	-	-	-	-	-	69	64	92
La	2340	14	0.58	1610	360	22	1310	76	5.8
Ce	6086	21	0.35	4990	1200	24	5010	400	8
Pr	719	24	3.3	710	240	34	797	86	11
Nd	2850	210	7.3	2770	830	30	3360	350	11
Sm	479	14	2.9	450	130	29	648	56	8.6
Eu	113.1	2	1.8	111	21	19	126.3	5.6	4.4
Gd	437	12	2.7	410	110	27	558	45	8.1
Tb	59	1.8	3.1	57	16	28	165	14	8.5
Dy	304	7.4	2.4	295	75	25	379	32	8.4
Ho	58.5	2.2	3.8	56	15	26	68.3	4.8	7
Er	178.2	6.9	3.9	169	42	24	201	11	5.5
Tm	25.87	0.51	2	24.3	6.1	25	25.4	1.3	5.3
Yb	177.9	2	1.1	166	38	23	162.4	4.1	2.5
Lu	25.87	0.23	0.89	24.4	4.9	20	21.559	0.074	3.4
Pb	-	-	-	-	-	-	9.33	0.79	8.4
Th	922.3	1.7	0.18	710	150	22	314.4	8.9	2.8
U	-	-	-	-	-	-	243	62	26

*Concentrations and standard deviation (2σ) are in ppm. RSD is reported in %.

Table 3 (cont'd): Trace-element concentrations of titanite crystals.*

	Mount Princeton Batholith		
Element	C_t	SD	RSD
Sc	15.6	3	19
Rb	-	-	-
Sr	-	-	-
Y	1300	250	19
Ba	-	-	-
La	1099	72	6.5
Ce	3460	270	7.8
Pr	578	41	7.1
Nd	2350	96	4.1
Sm	459	18	3.9
Eu	40	11	28
Gd	391	27	6.9
Tb	55.2	7	13
Dy	289	50	17
Ho	55	10	19
Er	162	33	20
Tm	22.9	5	22
Yb	148	30	20
Lu	20.6	4.3	21
Pb	-	-	-
Th	78.1	8.3	11
U	-	-	-

*Concentrations and standard deviation (2σ) are in ppm. RSD is reported in %.

Table 4: Trace-element concentrations in volcanic groundmass*

	Ammonia Tanks Member			Tiva Canyon Member†			Pagosa Peak Dacite†		
Element	C_g	SD	RSD	C_g	SD	RSD	C_g	SD	RSD
Sc	3.03	0.37	12	7	4.9	70	2.5	1.7	70
Rb	202	24	11	230	130	58	340	190	58
Sr	6.45	0.29	9.1	166	93	56	168	94	56
Y	9.6	2.8	30	17	14	83	8.8	7.3	83
Ba	5.8	2.5	44	450	280	62	570	350	61
La	5.5	6.7	120	16	17	106	16	17	106
Ce	16	13	81	40	27	69	29	20	69
Pr	1.6	1.8	117	4.3	3.7	86	2.2	1.9	86
Nd	5	5.7	114	16	13	80	6.5	5.2	80
Sm	1.1	1.2	106	2.8	2.1	76	0.91	0.69	76
Eu	0.028	0.026	91	0.48	0.44	91	0.26	0.24	91
Gd	1.2	1.2	104	2.8	2.2	78	1.07	0.84	78
Tb	0.21	0.21	100	0.76	0.56	74	0.26	0.19	74
Dy	1.3	1.3	98	1.7	1.1	67	0.63	0.42	67
Ho	0.28	0.28	97	0.31	0.24	76	0.13	0.1	76
Er	0.98	0.99	100	0.98	0.69	70	0.49	0.34	70
Tm	0.16	0.16	99	0.12	0.1	82	0.078	0.064	82
Yb	1.1	1.1	100	0.81	0.59	73	0.63	0.46	73
Lu	0.17	0.17	99	0.119	0.1	84	0.115	0.097	84
Pb	6.8	3.3	49	29	21	73	35	26	73
Th	8.6	3.7	43	6.9	5	73	11	8.1	73
U	4.4	3.2	74	4.1	3.9	94	11	11	94

*Concentrations and standard deviation (2σ) are in ppm. RSD is reported in %.

†Error calculated using the average relative standard deviations of the Ammonia Tanks, Bonanza Rhyolite and Peach Springs Tuff. See text for details.

Table 4 (cont'd): Trace-element concentrations in volcanic groundmass*

	Fish Canyon Tuff†			Bonanza Rhyolite			Peach Springs Tuff		
Element	C_g	SD	RSD	C_g	SD	RSD	C_g	SD	RSD
Sc	6.7	4.7	70	7	7.5	107	3.3	3	91
Rb	113	65	58	240	250	106	3.6	2	56
Sr	540	300	56	58	54	93	150	95	65
Y	8.7	7.2	83	14	18	130	1.11	1	90
Ba	910	550	61	79	64	80	10.4	6.1	59
La	9	10	106	15	17	118	2.8	2.2	78
Ce	28	12	69	29	27	92	5.8	1.8	31
Pr	1.9	1.6	87	3.4	2.9	85	0.66	0.37	55
Nd	6.3	5.1	80	10.2	7.7	76	2	1	52
Sm	1.08	0.82	76	1.6	1	62	0.3	0.16	51
Eu	0.44	0.4	91	0.15	0.12	80	0.02	0.021	103
Gd	1.16	0.91	78	1.8	1.3	70	0.32	0.19	59
Tb	0.31	0.23	74	0.25	0.15	61	0.039	0.021	54
Dy	0.72	0.48	67	1.29	0.73	57	0.172	0.07	41
Ho	0.15	0.11	76	0.28	0.17	63	0.032	0.022	69
Er	0.5	0.35	70	0.96	0.6	63	0.126	0.063	50
Tm	0.074	0.061	82	0.145	0.096	66	0.023	0.018	78
Yb	0.55	0.4	73	1.06	0.69	65	0.27	0.15	57
Lu	0.091	0.076	84	0.16	0.12	75	0.05	0.04	79
Pb	20	15	73	9.2	8.1	88	8.5	6.9	82
Th	6.2	4.6	73	16	15	94	5.9	4.8	82
U	3.5	3.3	94	3.6	4.4	122	1.07	0.93	87

*Concentrations and standard deviation (2σ) are in ppm. RSD is reported in %.

†Error calculated using the average relative standard deviations of the Ammonia Tanks, Bonanza Rhyolite and Peach Springs Tuff. See text for details.

Table 4 (cont'd): Trace-element concentrations in volcanic groundmass*

	Wall Mountain Tuff†		
Element	C_g	SD	RSD
Sc	6.8	4.8	70
Rb	250	150	58
Sr	74	41	56
Y	18	15	83
Ba	370	230	61
La	14	15	106
Ce	48	33	69
Pr	4.1	3.5	86
Nd	15	12	80
Sm	2.9	2.2	76
Eu	0.46	0.42	91
Gd	2.8	2.2	78
Tb	0.79	0.58	74
Dy	1.8	1.2	67
Ho	0.35	0.26	76
Er	1.07	0.75	70
Tm	0.14	0.12	82
Yb	0.91	0.67	73
Lu	0.14	0.12	84
Pb	30	22	73
Th	12.8	9.4	73
U	10.4	10	94

*Concentrations and standard deviation (2σ) are in ppm. RSD is reported in %.
†Error calculated using the average relative standard deviations of the Ammonia Tanks, Bonanza Rhyolite and Peach Springs Tuff. See text for details.

Table 5: Major-element compositions of selected titanite grains*

	Ammonia Tanks			Tiva Canyon			Peach Springs Tuff		
	Wt. %	SD	RSD	Wt. %	SD	RSD	Wt. %	SD	RSD
SiO_2	28.64	1.06	3.7	28.30	0.86	3.04	29.10	0.58	2.0
Ce_2O_3	1.24	0.28	22.6	1.61	0.30	18.6	1.60	0.12	7.5
Al_2O_3	1.44	0.32	22.2	1.38	0.26	18.8	1.61	0.06	3.7
CaO	23.64	1.06	4.5	23.76	0.60	2.52	24.46	0.66	2.7
FeO	2.96	0.44	14.9	2.34	0.46	19.7	2.63	0.20	7.6
TiO_2	35.08	1.68	4.8	36.50	0.84	2.30	35.84	0.84	2.3
Total	93.26			94.07			95.40		

	Wall Mountain Tuff			Mount Princeton Batholith		
	Wt. %	SD	RSD	Wt. %	SD	RSD
SiO_2	29.68	0.42	1.4	29.50	0.66	2.2
Ce_2O_3	0.47	0.44	93.6	0.83	0.62	74.7
Al_2O_3	3.35	0.46	13.7	0.66	0.36	54.5
CaO	25.82	0.58	2.2	25.97	0.92	3.5
FeO	1.95	0.20	10.3	1.57	0.50	31.8
TiO_2	34.11	0.52	1.5	38.98	1.06	2.7
Total	95.41			97.54		

* Standard deviation (2σ) is in ppm. RSD is reported in %.

Table 6: Titanite/groundmass partitioning values for volcanic titanite crystals*

	Ammonia Tanks Member			Tiva Canyon Member†			Pagosa Peak Dacite†		
Element	C_t/C_g	SD	RSD	C_t/C_g	SD	RSD	C_t/C_g	SD	RSD
Sc	25.3	4.1	16	14.2	9.5	67	18	14	77
Rb	0.236	0.035	15	0.16	0.11	70	0.039	0.026	66
Sr	1.31	0.62	48	0.43	0.49	112	0.5	0.3	61
Y	1920	640	33	800	660	82	870	730	84
Ba	11	16	147	0.35	0.29	84	0.18	0.16	88
La	370	460	122	150	150	101	200	210	106
Ce	570	480	83	240	170	69	370	270	73
Pr	1000	1200	119	410	360	87	690	550	80
Nd	1300	1500	115	540	420	78	920	750	82
Sm	1700	1900	107	800	570	71	1230	940	76
Eu	1600	1500	93	580	550	95	610	580	95
Gd	1500	1600	105	710	540	76	810	710	78
Tb	3200	3200	101	830	630	76	1130	830	73
Dy	1400	1400	99	1000	620	63	1100	760	69
Ho	1200	1200	99	900	630	70	1000	760	77
Er	940	950	101	730	470	64	810	590	72
Tm	700	700	100	640	510	80	670	560	83
Yb	520	520	101	490	350	73	510	380	73
Lu	370	370	100	350	580	79	340	320	94
Pb	1.35	0.73	54	0.42	0.46	109	0.19	0.15	79
Th	27	12	45	22	16	74	25	19	76
U	9	6.7	74	6.9	6.5	95	9	8.7	96

* Standard deviation (2σ) is in ppm. RSD is reported in %.
†Partitioning values calculated using Monte Carlo simulation. See text for details.

Table 6 (cont'd): Titanite/groundmass partitioning values for volcanic titanite crystals*

	Fish Canyon Tuff†			Bonanza Rhyolite			Peach Springs Tuff		
Element	C_t/C_g	SD	RSD	C_t/C_g	SD	RSD	C_t/C_g	SD	RSD
Sc	5.5	3.8	70	17	18	107	31	30	98
Rb	0.056	0.038	67	0.032	0.051	160	1.13	0.69	61
Sr	0.154	0.087	57	0.28	0.28	99	0.2	0.18	94
Y	780	650	83	900	1200	129	10200	9800	96
Ba	0.072	0.047	65	1.09	0.89	81	4.4	2.9	66
La	320	360	110	240	290	118	1070	950	88
Ce	580	390	66	470	430	92	2000	1000	50
Pr	720	610	64	620	530	85	2800	1800	67
Nd	850	670	79	800	610	76	3900	2400	63
Sm	910	670	74	1010	640	63	5600	3400	60
Eu	360	330	91	420	330	80	6300	6900	110
Gd	790	610	77	840	590	70	4700	3100	67
Tb	880	640	73	2000	1200	61	12000	7500	62
Dy	900	570	64	1000	560	57	6800	3400	50
Ho	820	600	73	860	540	63	6700	5100	76
Er	730	520	71	690	430	63	4600	2800	61
Tm	650	530	81	540	360	66	2800	2400	85
Yb	550	390	71	400	260	65	1320	880	67
Lu	430	370	85	290	220	75	790	690	88
Pb	0.24	0.18	73	0.93	0.83	89	0.78	0.71	92
Th	44	33	74	26	25	94	70	37	94
U	30	28	95	27	33	122	33	32	97

* Standard deviation (2σ) is in ppm. RSD is reported in %.
†Partitioning values calculated using Monte Carlo simulation. See text for details.

Table 6 (cont'd): Titanite/groundmass partitioning values for volcanic titanite crystals*

	Wall Mountain Tuff†		
Element	C_t/C_g	SD	RSD
Sc	18	13	73
Rb	0.014	0.011	78
Sr	0.95	0.75	79
Y	490	400	82
Ba	0.21	0.19	89
La	160	160	103
Ce	180	120	69
Pr	350	320	91
Nd	470	360	77
Sm	540	420	77
Eu	420	390	93
Gd	470	360	77
Tb	510	400	78
Dy	530	380	71
Ho	500	370	73
Er	430	300	70
Tm	390	340	88
Yb	330	250	75
Lu	270	230	85
Pb	1.15	0.95	82
Th	21	16	76
U	12	11	96

* Standard deviation (2σ) is in ppm. RSD is reported in %.
†Partitioning values calculated using Monte Carlo simulation. See text for details.

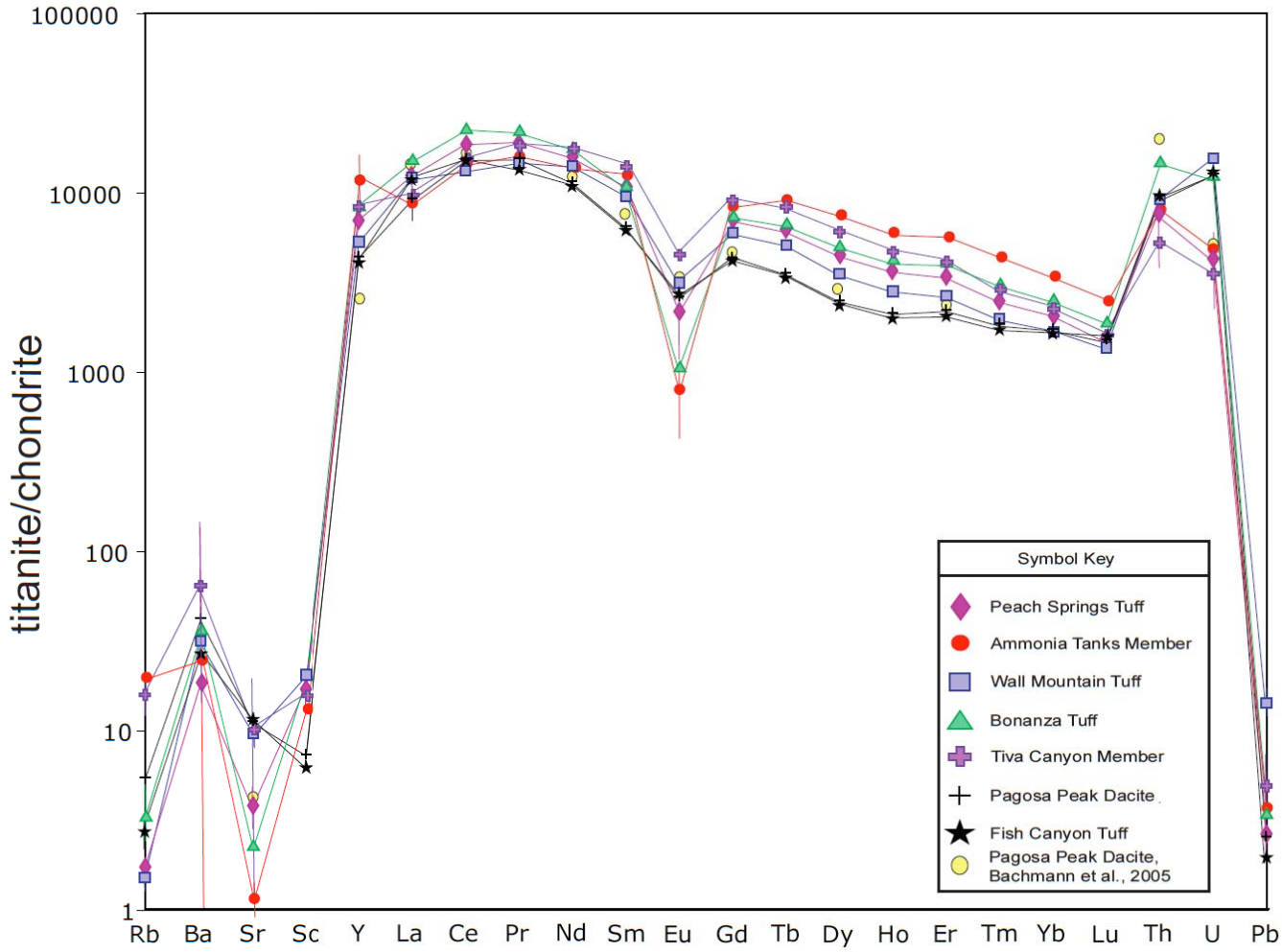

Figure 4: Average trace-element concentrations in titanite crystals in dacitic to rhyolitic volcanic rocks from the western United States. Concentrations are normalized to C1 chondrite of Sun and McDonough (1989). Elements are ordered by increasing valency. In most cases, error bars are smaller than the symbols.The REEs, Y, Th and U are enriched up to three orders of magnitude relative to Rb, Ba, Sr, Sc and Pb. Error bars are 2 sigma.

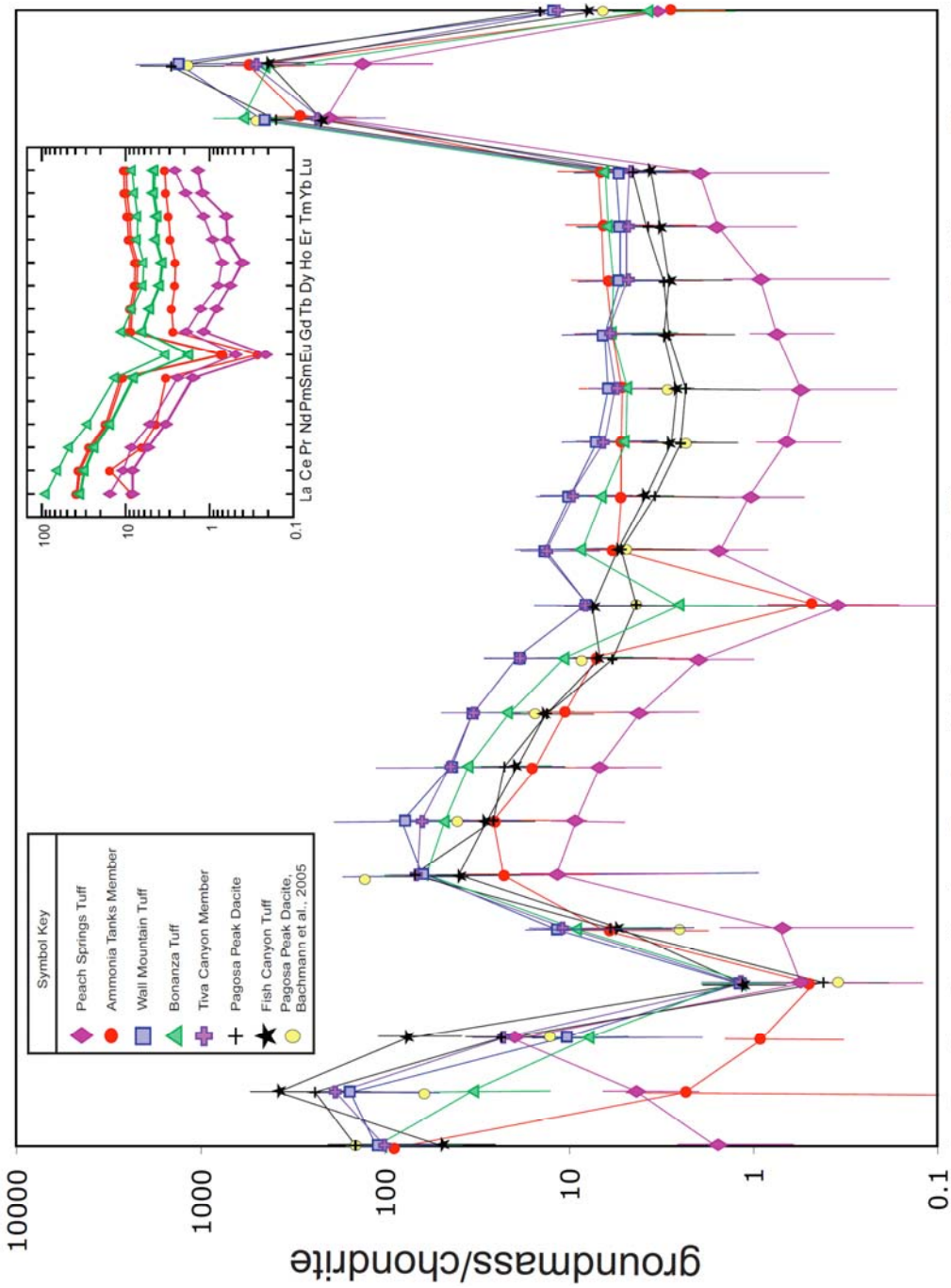

Figure 5: Trace-element concentrations in groundmass of dacitic to rhyolitic volcanic rocks from the western United States. Concentrations are normalized relative to C1 chondrite of Sun and McDonough (1989).The inset shows the results of replicate analyses of the rare earth elements from the Bonanza Tuff, Ammonia Tanks Member, and Peach Springs Tuff. Error bars are two sigma.

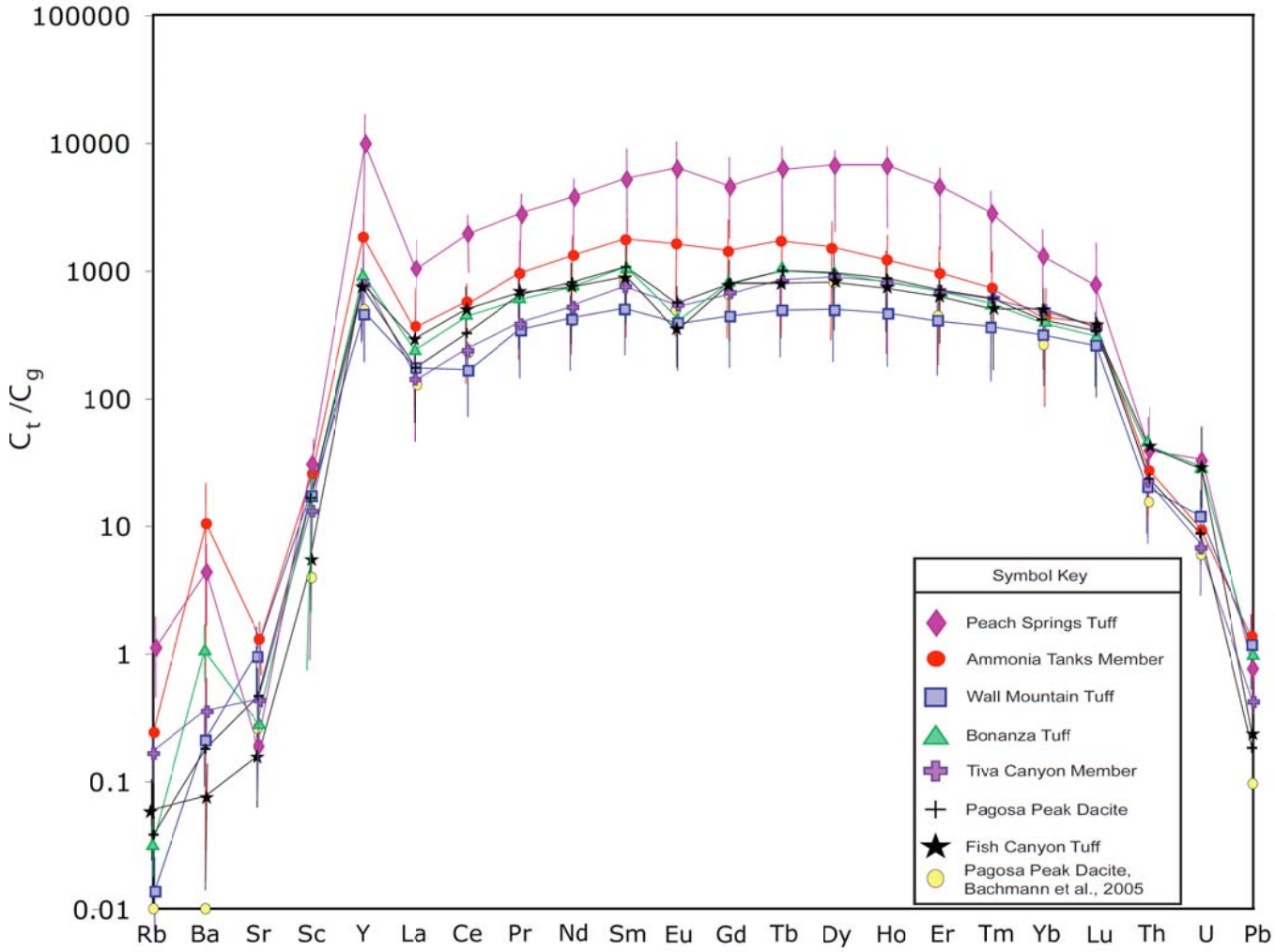

Figure 6: Titanite/groundmass trace-element partitioning values of dacitic to rhyolitic volcanic rocks from the western United States. For most elements, partitioning values vary over an order of magnitude between rock units. With the exception of Rb, Ba, Sr, Sc and Pb most trace elements are compatible in titanite relative to the groundmass. The high partitioning values of the REEs and Y make titanite an important mineral in the trace-elemet budgets of volcanic and plutonic rocks. Error bars are 1 sigma.

Data Quality and Reproducibility of Results

Results of trace-element concentrations in titanite crystals between replicates were consistent. Each titanite sample (with the exception of the Wall Mountain Tuff) had 2-3 replicates. Due to the low modal abundance of titanite crystals, the rarity of inclusion-free titanite crystals and the small size of the crystals (100 microns or less), only one replicate of Wall Mountain Tuff titanite was analyzed. Most samples had relative standard deviations (RSDs) below 20%. Because analyzed titanite crystals were inclusion-free, inter-sample variation was likely caused by error from weighing the crystals or incomplete dissolution during sample preparation. Analyzing multiple titanite crystals per replicate yielded an average crystal composition, most likely averaging the effect of zoning.

Due to the difficulty of accurately separating clean groundmass samples, three of the seven groundmass replicates were prepared and analyzed three times, whereas the remaining four were prepared and analyzed only once. The replicates that were analyzed three times were from the Ammonia Tanks Member, Bonanza Tuff, and Peach Springs Tuff (inset, Fig. 5). Two of the replicates from each of the three samples were run during the same collection period, whereas another was analyzed separately. Standard deviations of the four groundmass samples that were analyzed only once were determined using a weighted average of the three replicates of the Ammonia Tanks Member, Bonanza Rhyolite and Peach Springs Tuff groundmasses. The two replicates run during the same collection period yielded similar concentrations and were weighted 0.25 each, whereas the other value was weighted 0.5. Analyses of trace elements in groundmasses had much greater standard deviations than the analyses of titanite crystals. Between the samples with three replicates, relative standard

deviations were typically greater than 50%. Despite the range in concentrations between replicates of the Ammonia Tanks Member, Bonanza Rhyolite and Peach Springs Tuff (inset, Fig. 5), the similarity of the shapes of the groundmass REE curves indicates that the shapes of the partitioning curves (Fig. 6) are robust.

Two main factors contribute to the large standard deviations of the groundmass samples. First, ICP-MS analyses are less accurate at lower concentrations. For example, analyses of the REEs in titanite had average relative standard deviations less than 20%. However, low-concentration elements like Sr and Ba had RSDs upwards of 80% for some samples. Despite dissolving large quantities of groundmass for analysis, after dilution for analysis, many of the elements were in the 1-10 ppb range, near the low end of ICP-MS detection.

The second source of variance in groundmass analyses was the lack of a constant flow through the nebulizer on the ICP-MS. Despite filtering the samples, some particulate matter made it through to the nebulizer since large volumes of groundmass were dissolved in small volumes of acid. This caused flow through the nebulizer to vary from replicate to replicate, skewing the results. Reduced flow on the ICP-MS is monitored using ^{115}In ratios. During our analysis, the ^{115}In ratios for the titanite samples and standards were all very near 1. However, the ^{115}In ratios for many of the groundmass analyses were much lower than 1 (0.75-0.85) meaning less ^{115}In was getting through the system to the detector, indicating a clogged nebulizer. The count intensity of a sample is divided by the ^{115}In ratio as a way to correct for changes in flow; however, this correction cannot account for all the error caused by changes in flow, which can result in a range of reported concentrations.

Standard deviations of partitioning values for the multiple-groundmass replicate samples of the Ammonia Tanks Member, Bonanza Rhyolite and Peach Springs Tuff (C_t/C_g, see discussion below) were determined using the error propagation formula:

$$\left(\frac{\sigma_{C_t/C_g}}{C_t/C_g}\right)^2 = \left(\frac{\sigma_{C_t}}{C_t}\right)^2 + \left(\frac{\sigma_{C_g}}{C_g}\right)^2 \quad (2)$$

where σ is the standard deviation, and C_t and C_g represent the concentrations of an element in titanite and groundmass, so that C_t/C_g is the partitioning value of that element. This method of error propagation relies on two assumptions. First, it must be assumed that the two variables (C_t and C_g) are uncorrelated. This assumption is being made because the small sample size makes accurately determining a correlation coefficient implausible. The second assumption is that the variance is normally distributed around the mean values of the concentrations. Because of the small number of replicates, it is not possible to quantitatively determine whether the variance is normally distributed, so this assumption must be held as true.

A Monte Carlo simulation was used to estimate the partitioning values and standard deviations for those samples in which only one groundmass replicate was analyzed (Tiva Canyon Member, Pagosa Peak dacite, Fish Canyon Tuff and Wall Mountain tuff). For each element in a sample, a simulated set of titanite concentrations was created by generating a 4000-value vector of random numbers with a mean and standard deviation equal to the values observed in the titanite. To attain the partitioning values and standard deviations, this vector was divided by a vector of equal length for the groundmass, using the individual concentration value measured as the mean for the simulation. Partitioning values that were negative (less than 0.5%) were omitted from the data set.

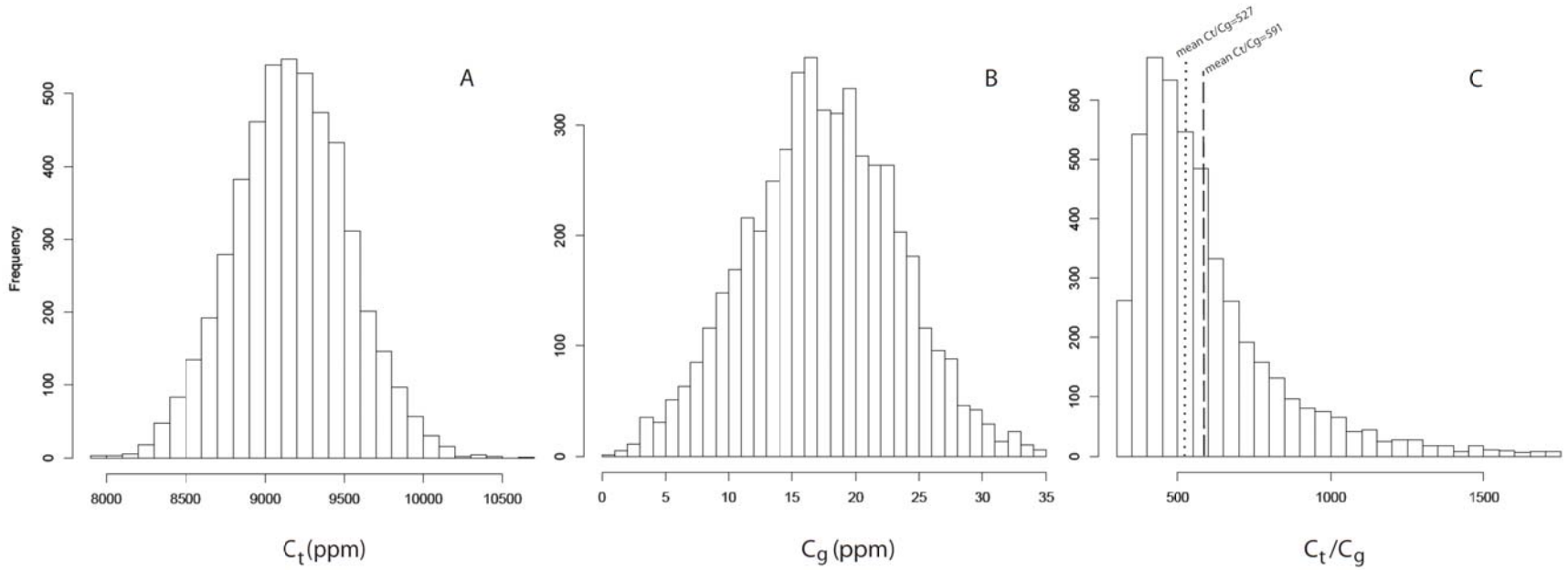

Figure 7: Example Monte Carlo simulations for Ce from the Fish Canyon Tuff. (A) and (B) are histograms of 4000 count vectors of random values averaged around the mean C_t and C_g values. (C) shows a histogram of the vector resulting from dividing vector C_t by C_g. Because of the right skew of the distribution, the average C_t/C_g value (dashed line) is around 10% higher than if the C_t/C_g value was calculated by simply dividing the mean values for C_t and C_g (dotted line).

The average partitioning values and their standard deviations were then calculated from the partitioning value vectors. Dividing the normally distributed vector of high titanite concentrations by the normally distributed vector of low concentration groundmass does not yield a normally distributed vector of partitioning values. Instead, the partitioning values are skewed to the right (high values; Fig. 7). Because of the skew, average partitioning values were about 10% higher than they would have been had the value been calculated by dividing the average titanite by the average groundmass concentrations used as inputs parameters for the Monte Carlo. Despite the skew, standard deviations are approximated to be normally distributed, and are useful in understanding the magnitude of possible variation in partitioning values.

IV. DISCUSSION

Understanding 1) the range of trace-element partitioning values for titanite in silicic magma systems, 2) the factors affecting trace element partitioning, and 3) differences between trace element concentrations in titanite from varied petrologic settings are necessary for developing models for the formation of plutonic and volcanic rocks, and understanding the petrogenetic connections between plutonic and volcanic rocks. The following discussion aims to identify the factors that exert the greatest control on trace-element partitioning into titanite, and to provide explanations for the differences observed between plutonic and volcanic titanite.

Integrity of the Groundmass Data

There are two concerns regarding the integrity of the groundmass data reported in this study. First, the Peach Springs Tuff groundmass is visibly altered which distinguishes it from the other samples in this study. Alteration resulted in a low totals and anomalously low SiO_2, Na_2O and K_2O, and high Al_2O_3 for the Peach Springs Tuff. Consequently, the partitioning values determined for the Peach Springs Tuff are likely not accurate representations of titanite/groundmass partitioning behavior of the REEs.

A second concern about the trace element analyses of groundmass is that because the concentrations of trace elements in the groundmass are low, small amounts of trace minerals could have a large effect on groundmass analyses. Although careful attention was paid to select clean groundmass separates for analysis, it is possible that microlytic trace minerals or

contaminant phenocrysts could have been dissolved with the groundmass. The most obvious concern regarding contamination is with the Fish Canyon Tuff groundmass, which has a positive Eu anomaly (Fig. 5). Feldspars— which partition Eu^{2+} into their Ca site— are the most likely cause of contamination. Whereas SEM analysis of the Fish Canyon Tuff groundmass indicated <10% microlytic minerals, feldspar crystals were similar in color and texture to the groundmass and could have been unwittingly added to the groundmass separate.

A simple mass-balance model helps determine the amount of feldspar contamination needed to cause the Eu anomaly in the Fish Canyon Tuff groundmass and evaluate the possibility of significant contamination. Fish Canyon Tuff plagioclase REE concentrations from Bachmann (2005) were subtracted from the groundmass values in amounts ranging from 1-20 weight % (Fig. 8). The modeling indicates that approximately 15 weight % plagioclase could be responsible for the positive Eu anomaly. However, careful inspection of groundmass under cross-polarized microscope prior to dissolution makes it unlikely that 15% plagioclase as phenocrysts or microlites were present in the groundmass. Rather, it is more likely that the positive anomaly in the Fish Canyon Tuff groundmass is real. Consequently,

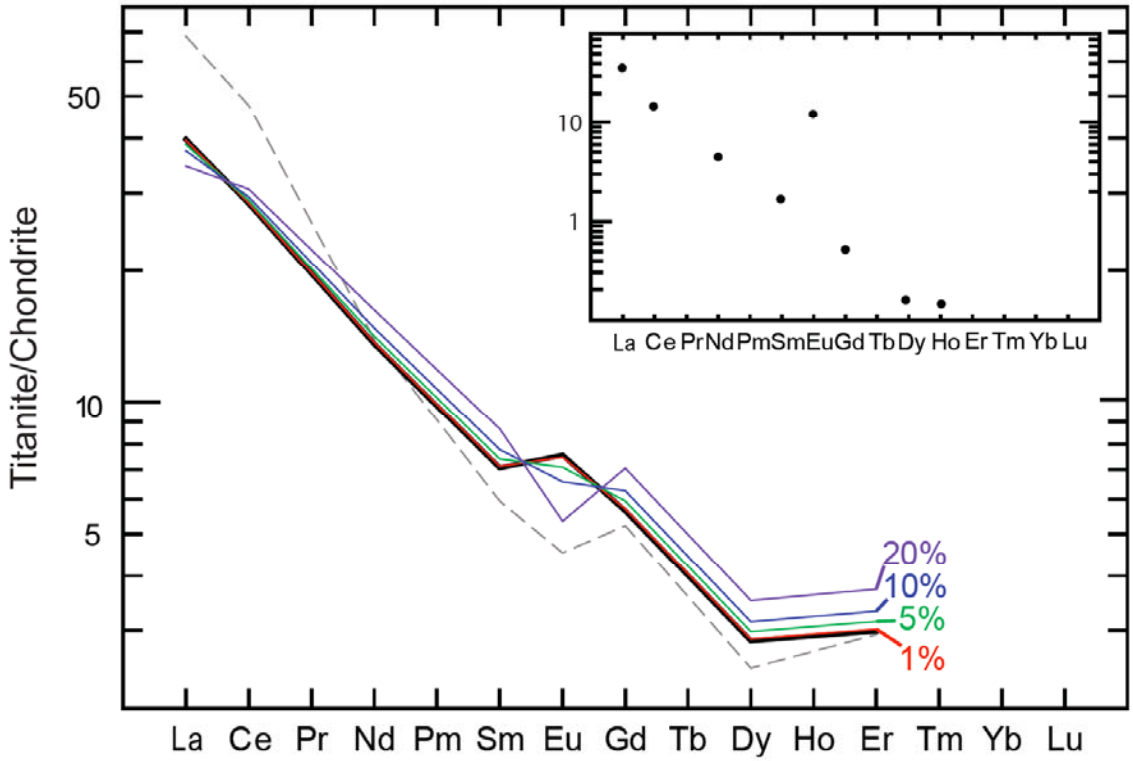

Figure 8: Model of plagioclase contamination of Fish Canyon Tuff groundmass. Values are normalized to Sun McDonough (1989). The black line is the measured value for the Fish Canyon Tuff, demonstrating a positive europium anomaly. Colored lines represent groundmass compositions if plagioclase contamination of 20%, 10%, 5%, 1% wt% are removed from the groundmass. Dashed line represents the composition of Pagosa Peak dacite groundmass from Bachmann (2005). Plagioclase composition is the average Fish Canyon Tuff plagioclase from Bachmann (2005), shown in insert.

the range of partitioning values determined for the Fish Canyon Tuff and all other samples (except the Peach Springs Tuff) are interpreted to be reflective of differences between the magmatic systems.

Trace Element Partitioning

Trace-element titanite/groundmass partitioning values in silicic volcanic systems measured in this study range over an order of magnitude and are likely affected by lattice strain, melt polymerization, the water content of the melt, temperature and pressure (Watson 1976, Hart and Davis 1978, Takahashi 1978, Mahood and Hildreth 1983, Blundy and Wood 1994, Prowatke and Klemme 2005). This study focuses on the impact of lattice strain and melt polymerization because water content was beyond the scope of the investigation, and temperature and pressure are demonstrated to have little impact on partitioning (Hart and Davis 1978, Takahashi 1978, Mahood and Hildreth 1983, Prowatke and Klemme 2005).

An increase in water content decreases melt polymerization, offers more ligands for trace metal complexing (Lipman 1971, Hildreth 1979, Mahood and Hildreth 1983) and decreases the temperature of crystallization. Although no quantitative data are available, the effects of varied water content might be recorded by the partitioning behavior of titanite. For example, the Fish Canyon Tuff magma system was wet (5 wt. % H_2O), existed at relatively low temperatures near 760 ˚C (Johnson and Rutherford 1989, Lipman 2007, Bachmann et al. 2008) and had low partitioning values. Conversely, the Ammonia Tanks Member was a relatively dry (1-2 wt% H_2O) magma (Lipman 1966, Christiansen et al. 1977) that existed at temperatures around 820 ˚C (Flood et al. 1989, Bindeman et al. 2006) and had much higher partitioning values. Green and Pearson (1986) studied the effect of pressure on titanite's partitioning behavior from 7.5 to 30 kbar and 900 to 1120˚C (Fig. 9). They determined that

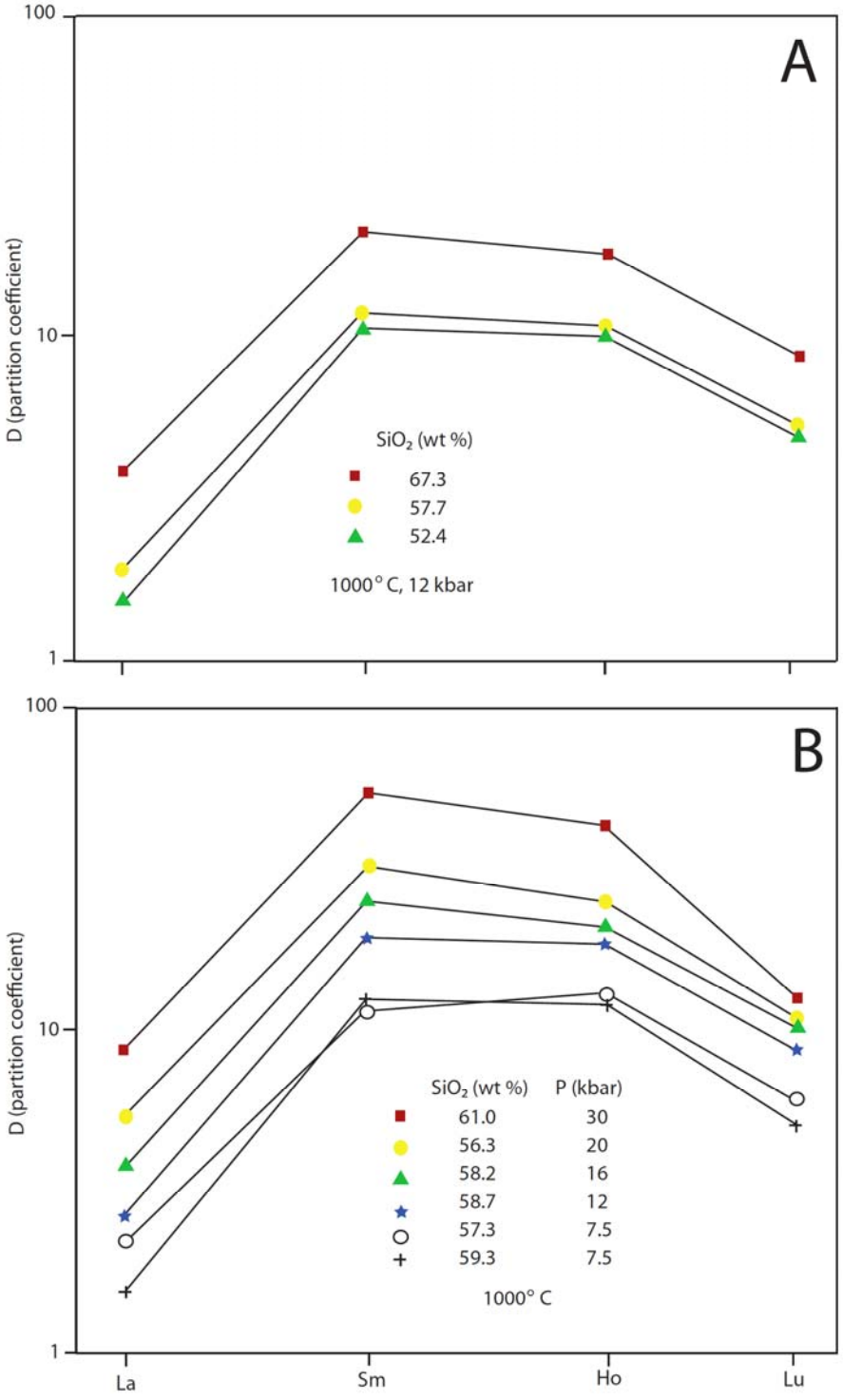

Figure 9: (A) Effect of melt composition on partitioning of REEs into titanite, showing a positive correlation between the SiO_2 content and partition coefficients of REEs. (B) Positive correlation between pressure and partition coefficients of REEs between titanite crystals and silicate melt. Adapted from Green and Pearson (1985).

increasing pressures increased the partitioning of REEs into titanite. However, pressure— as noticed by Prowatke and Klemme (2005)— is unlikely to affect titanite in cooler, more silicic systems that crystallized at lower pressures.

Lattice Strain

The substitution of the smaller trivalent REEs into the divalent Ca site cannot occur at high concentrations without straining the titanite crystal lattice. The lattice strain model (LSM) proposed by Brice (1975) and Blundy and Wood (1994) can be used to evaluate the effect of lattice rigidity on the partitioning of elements into a specific crystallographic site. LSMs are displayed on graphs of ionic radius versus the log of partitioning values. The LSM fits a non-weighted non-linear least squares regression to the equation:

$$D_i = D_0 \exp\left\{-4\pi E_M N_A \times \left[r_0(r_i - r_0)^2/2 + (r_i - r_0)^3/3\right]/RT\right\} \quad (3)$$

where D_o and r_o are the ideal partition coefficient and ionic radius (least strained radius, peak of the curve), D_i and r_i are the partition coefficient and ionic radius of cation *i*, E_M is the Young's modulus of the cation site, N_A is Avogadro's number, R is the gas constant and T is temperature in Kelvin. When available, the Shannon (1976) ionic radii of the 3^+ REEs in sevenfold coordination were used for the model. Not all REE's have a known sevenfold coordinated ionic radius; however, a plot of ionic radius of isovalent REEs in sevenfold coordination is roughly linear with atomic number, allowing for interpolation between known ionic radii. The LSM only holds for isovalent cations. Because of this, the divalent element Eu was omitted from the model.

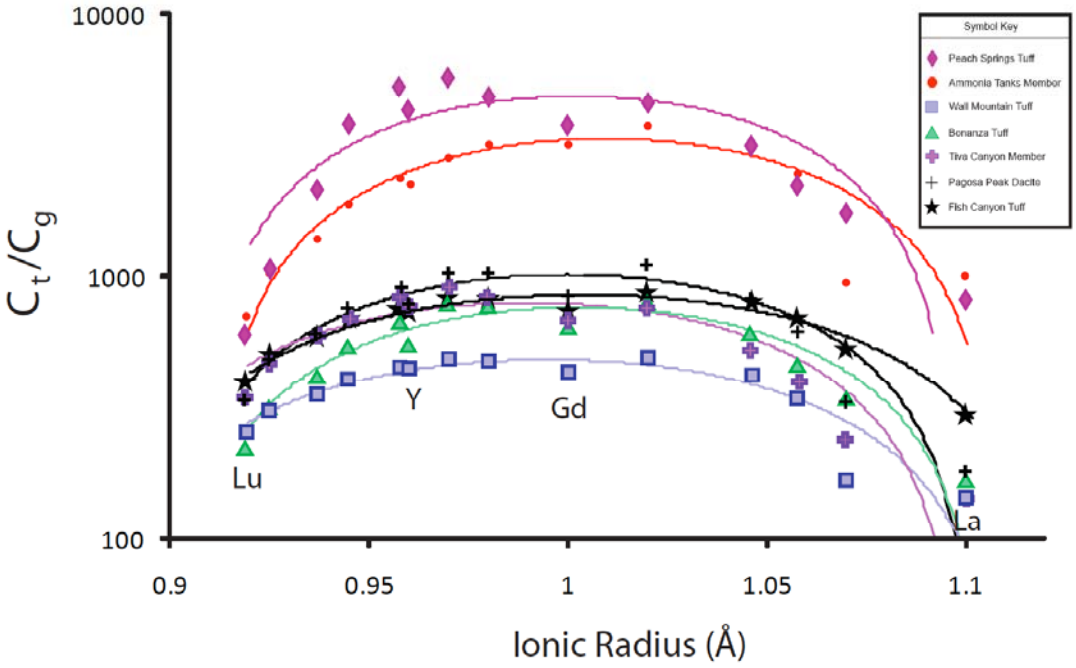

Figure 10: Results of lattice strain model, a method used to test the effect of crystal lattice rigidity on cation substitution. The fit of the model to the data suggests lattice strain plays a role in the partitioning of the REEs in titanite. D_o and r_o for each curve occur at the apex of the parabolas, and the Young's modulus is represented by the steepness of the curvature (steeper parabolas imply a more rigid lattice site). Fitting was performed using the graphical modelling program Origins.

The LSM (Table 7, Figure 10) returned consistent results between samples. The ideal ionic radius for most samples was near 100 pm, the ionic radius of Gd^{3+} in sevenfold coordination. Several factors must be considered when determining the applicability of the LSM to the understanding of partitioning. If the supply of partitioning elements from the melt is limited (which is likely the case with titanite, where melt concentrations of REEs – as estimated from groundmass concentrations, are orders of magnitude lower than in titanite), diffusion is likely to play an important role in the transport of an element to the crystal-melt boundary. Also, the coupled substitution of the REEs with Al and Fe adds complexity to interpreting lattice strain effects, as differing proportions of Al and Fe into the crystal lattice will cause varying degrees of expansion and contraction of the Ca-site.

Ignoring Al and Fe substitution decreases the accuracy of estimating the Young's modulus, which is done assuming that bond stress and strain are due only to the substitution of REEs into the Ca site. The magnitude of the Young's modulus is an indication of the rigidity of the lattice site. The size of the Young's moduli fitted to titanite in this study varied greatly from one sample to another (46.3-472.2 GPa), which may reflect the impact of ignoring the other substitutions. However, the average Young's modulus suggests a rigid lattice site, and compares favorably to the modulus determined by Olin 2010 (approximately 200 GPa).

Melt Polymerization

Along with lattice strain, melt polymerization is a useful parameter when considering the effect of melt composition on partitioning between titanite and groundmass (Watson 1976, Watson 1977, Mysen 1983, Prowatke and Klemme 2005, Prowatke and Klemme

Table 7: Results of Lattice Strain Modeling

	Ammonia Tanks Member	Tiva Canyon Member	Pagosa Peak Dacite	Fish Canyon Tuff	Bonanza Rhyolite	Peach Springs Tuff	Wall Mountain Tuff
T (°K)*	1093	1093	1033	1033	1067	1067	1033
D_o	3310	795	1010	853	763	4880	486
r_o (pm)	100.9	99.0	99.9	100.3	100.2	100.1	99.5
E_M (GPa)	46.3	287.3	187.6	76.8	244.8	472.2	115.0

*Temperatures from Flood et al. (1989) for Ammonia Tanks Member and Tiva Canyon Member, Whitney and Stormer (1985) for Pagosa Peak Dacite, Fish Canyon Tuff, Bonanza Rhyolite and Wall Mountain Tuff, and Pamukcu (2010) for Peach Springs Tuff.

2006). Melt polymerization is a descriptor of the structure of a melt, as defined by the degree of connectivity between silicon tetrahedra. As the polymerization of melt increases, the activity of trace element cations increases which increases the likelihood of their incorporation into crystalline phases (Watson 1976).

The aluminum saturation index (ASI) is a simple and effective metric to describe melt polymerization (Prowatke and Klemme 2005). ASI is defined as the molar proportion:

$$ASI = Al_2O_3/(CaO + K_2O + Na_2O) \quad (4)$$

Aluminum acts to help link silica tetrahedra, whereas metal cations act as network modifiers to decrease polymerization (Watson 1976, Mahood and Hildreth 1983).

The NBO/T is another useful descriptor of melt polymerization (Mysen 1983, Mysen 2004). NBO/T is a measure of the number of nonbridging oxygens compared to the number of tetrahedrally coordinated cations in a melt. NBO/T = 4 indicates a completely depolymerized melt, whereas NBO/T = 0 is a completely polymerized melt. The NBO/T value was calculated using an equation:

$$NBO/T = \frac{2(X_{CaO} + X_{MgO} + X_{FeO} + X_{MnO} + X_{Na_2O} + X_{K_2O})}{X_{SiO_2} + 2X_{Al_2O_3} + X_{TiO_2}} \quad (5)$$

modified from Jaeger and Drake (2000). For these calculations, the amount of Fe_2O_3 in the melt is negligible at the oxygen fugacities of the systems of interest (Kress and Carmichael 1991).

Increasing ASI values (and decreasing NBO/T) indicate increasing melt polymerization and consequent increases in the partitioning of REEs into titanite (Prowatke and Klemme 2005). The experiments of Prowatke and Klemme (2005) were performed in systems whose ASI values ranged from 0.115 to 0.768. The ASI values determined for the natural systems of our study were higher (1.01-1.19), implying a greater degree of melt

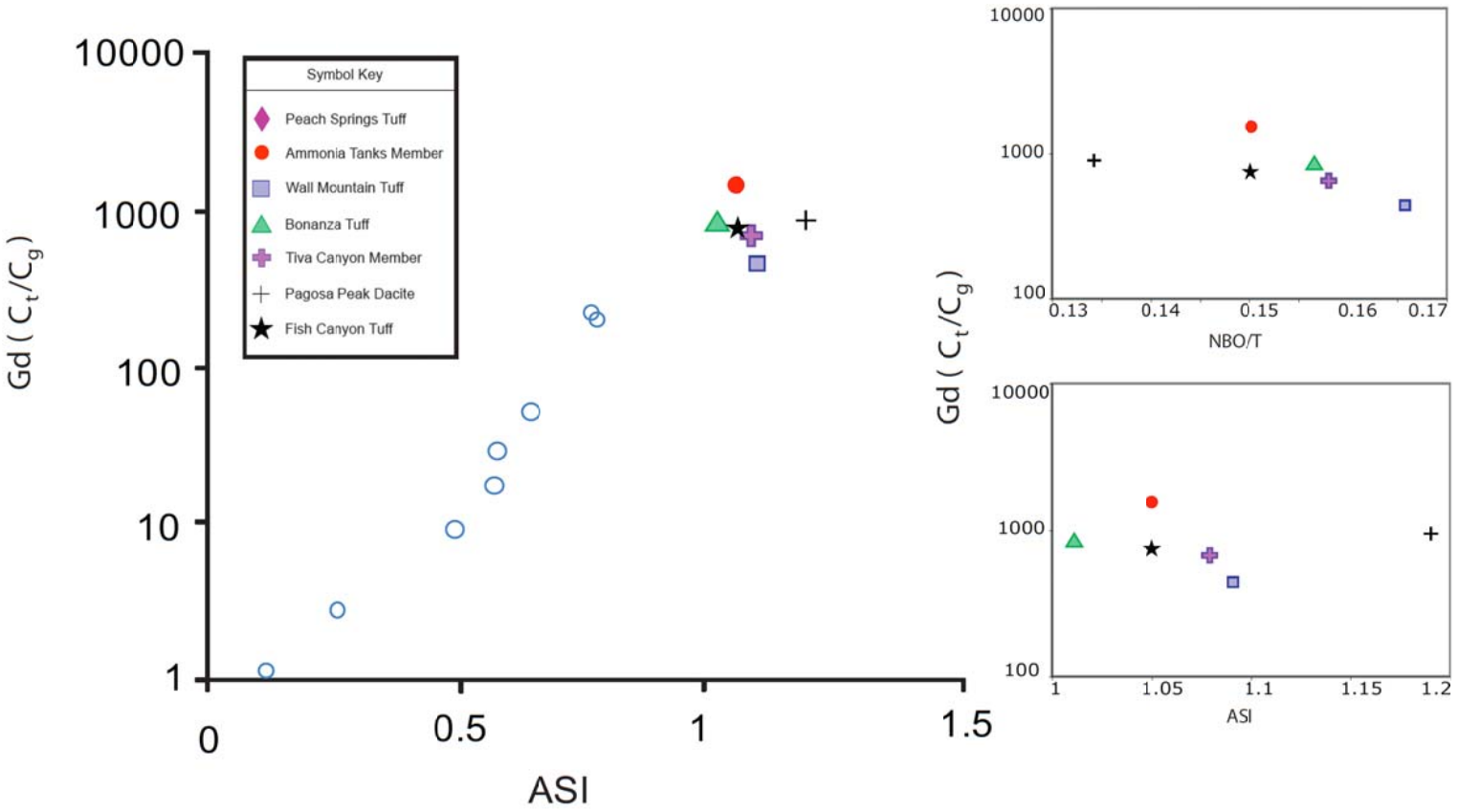

Figure 11: Aluminum saturation index (ASI, a measure of melt polymerization) of groundmass [ASI=Al_2O_3/(Na_2O+K_2O+CaO)] versus the average gadolinium partitioning values in complementary titanite. Open circles are data from experimental study by Prowatke and Klemme (2005). Inset compares NBO/T and ASI to Gd partitioning, showing no significant correlation between partitioning values and melt polymerization over the studied compositional range.

polymerization for our samples. There is no correlation between measures of melt polymerization and REE content (represented by plotting versus [Gd]; Fig. 11) for the samples in this study, probably because of the limited range of ASI. However, combining data from our study with the data from Prowatke and Klemme (2005) shows good agreement between the studies. Scatter in the data is likely due to differences in water pressure, volatile content, rates of cooling, melt composition, oxygen fugacity and temperature in the natural system that was not encountered in the controlled experimental studies of Prowatke and Klemme (2005).

Volcanic Versus Plutonic Titanite

Titanite crystals from plutonic and volcanic systems differ in their zoning, trace-element composition and trace-element substitution mechanisms. Understanding the differences between plutonic and volcanic titanite is useful in identifying the connections between plutonic and volcanic rocks.

Differences in growth zoning between plutonic and volcanic titanite suggest different environments of formation. Whereas growth zoning is distinct and finely banded in volcanic titanite, plutonic titanite typically exhibits thicker less pronounced growth zones (Fig. 12). Oscillations that might reflect diffusion controlled zoning can clearly be seen in the Ammonia Tanks member titanite (Fig. 12). Here, the initially high concentrations of REEs (bright regions) grade to lower concentrations (darker regions). Moving outward from the core of the crystal, the boundary between dark and light regions is sharp, indicating a period of no crystal growth allowing for re-equilibration of the melt-crystal interface. In plutonic titanite, the thicker and less distinct growth zoning is likely caused by thermal oscillations in

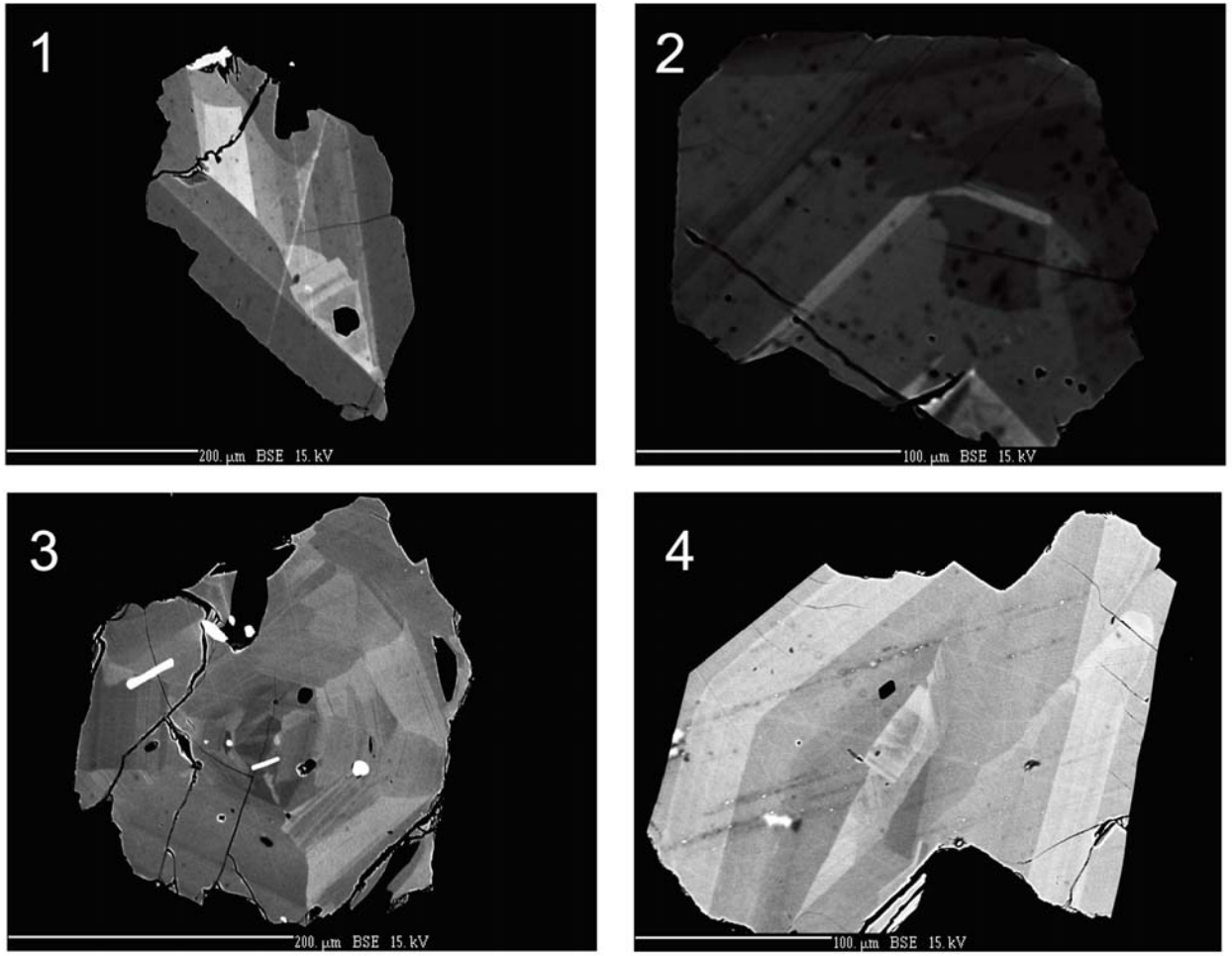

Figure 12: BSE images of zoning in titanite from several plutonic and volcanic rocks. BSE brightness is positively correlated with the REE+Y content of the crystal (Paterson and Stephens 1992, Vuorinen and Halenius 2005, McLeod et al. 2011). (1,2) Sector and minor growth zoning in titanites from the Mount Princeton batholith. Sector zoning in (3) Tiva Canyon Member titanites. The constrast in color between the light and dark zones is due to the preferential occurence of the REEs along the {100} sectors and the preference of Al and Fe along the {111} sectors. (4) Distinct oscillatory zoning in titanite from the Ammonia Tanks Member.

a near-solidus system. Dickinson (1996) and Johnson et al. (2010) describe a similar mechanism to explain Ba zoning in K-feldspar in plutonic rocks.

Plutonic and volcanic titanite crystals also display some clear differences in their trace element content—in particular the REEs (Fig. 13). With the exception of La, Ce, Eu, and Lu, plutonic titanite crystals generally have lower REE concentrations, and are most similar to Fish Canyon Tuff and Pagosa Peak dacite titanite crystals. The Fish Canyon Tuff and Pagosa Peak dacite are thought to be rejuvenated plutonic rocks (Bachmann et al., 2002), which may explain the similarity of their REE profiles to the plutonic titanite crystals, whereas the other volcanic rocks sampled are thought to have formed through down-temperature crystallization from a largely liquid magma. Lower REE concentrations in plutonic, Fish Canyon Tuff, and Pagosa Peak dacite titanite crystals could also be explained by competition with other trace-element bearing phases such as zircon, allanite, and amphibole. The similarity of trace-element concentrations of plutonic titanite and titanite from the Fish Canyon Tuff and Pagosa Peak dacite indicates that partitioning values of trace elements in the Fish Canyon magma system could be used for accurate plutonic trace-element fractionation modeling.

Trace-element substitutions into titanite involve a coupled substitution with major elements, and differences in the substitutions between plutonic and volcanic titanite strengthen the idea that they formed under different conditions. The mechanisms of substitution differ depending on the environment in which titanite is crystallizing. Mechanisms involving Al^{3+} and Fe^{3+} coupled substitutions into the Ti-octahedral site have been proposed for a range of magmatic and metamorphic systems (Ribbe 1982, Vuorinen and Halenius 2005). It is also possible to substitute Nb^{3+} and the other HFSEs into the Ti-site.

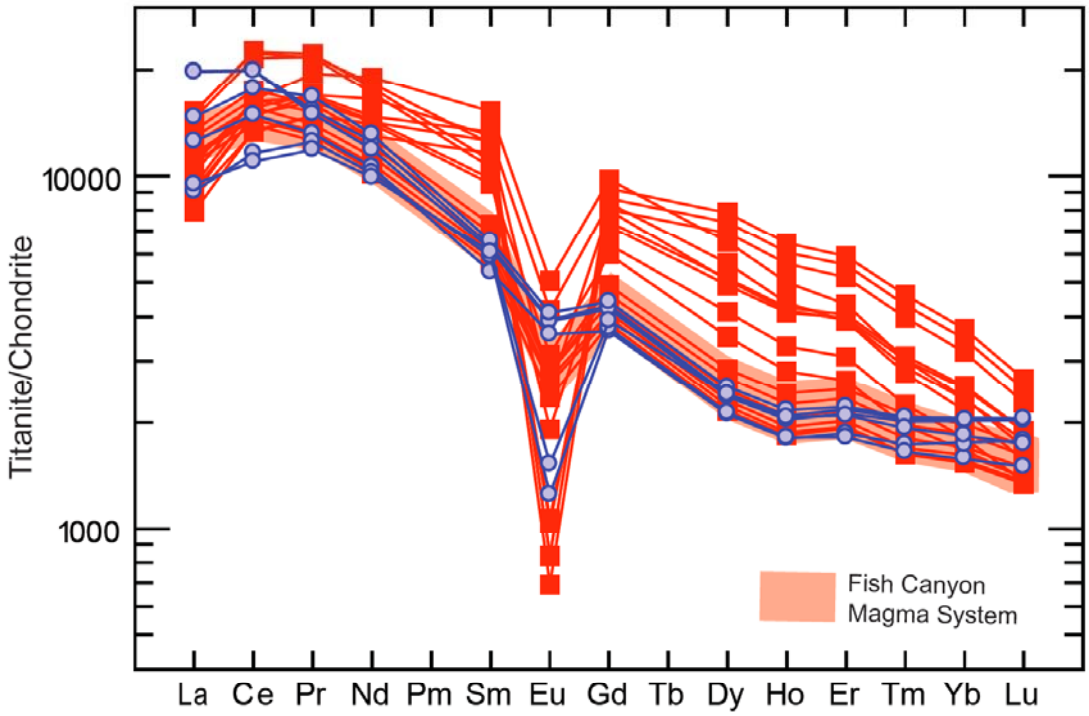

Figure 13: REE concentrations in titanites from volcanic (■) and plutonic (○) rocks. With the exception of La, Ce, Eu, and Lu, plutonic titanite crystals generally exhibit lower REE concentrations, and are most similar to Fish Canyon Tuff and Pagosa Peak dacite titanite crystals. The Fish Canyon Tuff and Pagosa Peak dacite are thought to be rejuvenated plutonic rocks (Bachman et al. 2002), which may explain the similarity of their REE profiles to the plutonic titanite crystals, whereas the other volcanic rocks sampled are thought to form through down-temperature crystallization from a largely liquid magma.

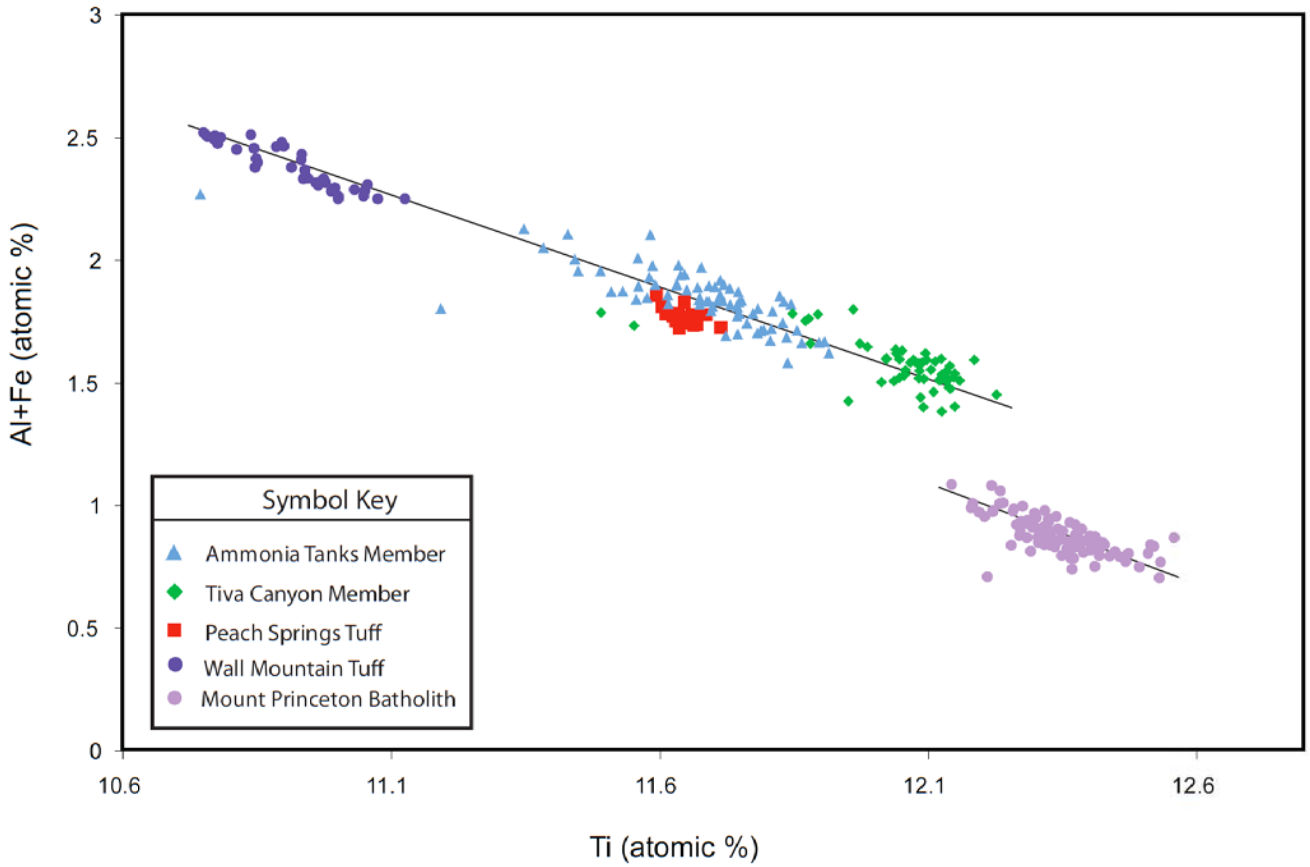

Figure 14: Atomic Ti versus Al + Fe compositions in titanite crystals. The negative slope demonstrates that Al^{3+} and Fe^{3+} substitute into the Ti^{4+} site to charge balance the REE^{3+} and Y^{3+} substitution in the Ca^{2+} site. Best fit lines are drawn through the volcanic and plutonic titanite. The difference between volcanic and plutonic titanite crystals is likely due to greater concentrations of niobium and other highly incompatible elements in the melt that plutonic titanite crystallizes from. Because Nb^{3+} is favored over Al^{3+} and Fe^{3+} in the crystal structure of titanite (Frost et al., 2000, Vourinen and Halenius, 2005), higher concentrations of Nb will correspond with lower concentrations of Al + Fe.

The titanite crystals studied here predominantly underwent the charge-balanced coupled substitution of Al^{3+} and Fe^{3+} for Ti^{4+}, and $REEs^{3+}$ and Y^{3+} for Ca^{2+}, resulting in a negative correlation between molar Al + Fe versus molar Ti in titanite (Fig. 14). It is also evident from figure 14 that data for titanite from the Mount Princeton Batholith has a similar slope but lower Al+Fe relative to the volcanic titanite. This is most likely due to a greater concentration of Nb available during the crystallization of plutonic titanite. Niobium is a very incompatible element that fits well into the Ti site in titanite. In systems that contain titanite, it is the major Nb-bearing phase and may prefer Nb to Al and Fe (Frost et al. 2000, Vourinen and Halenius, 2005). Because Nb is incompatible in most mineral phases, late-stage magmatic fluids are also enriched in Nb. Therefore, titanite that crystallizes from plutonic rocks where the melt-phase is more enriched in Nb will have greater concentrations of Nb than titanite that crystallizes from typical volcanic systems, decreasing the amount of Al and Fe required to charge compensate REE substitution.

Another difference between plutonic and volcanic titanite is the relationship between Eu anomalies and concentrations of the other REEs in titanite. Europium anomalies in the bulk rock and melt phase are traditionally interpreted as evidence of feldspar fractionation (Graham and Ringwood 1971). Greater differences between the actual and expected values of Eu (decreasing Eu/Eu*) imply more plagioclase fractionation, and enrichment of the other, more incompatible REEs in the melt. Eu/Eu* was calculated using the equation:

$$Eu / Eu^* = \frac{Eu_N}{\sqrt{Sm_N \bullet Gd_N}} \qquad (6)$$

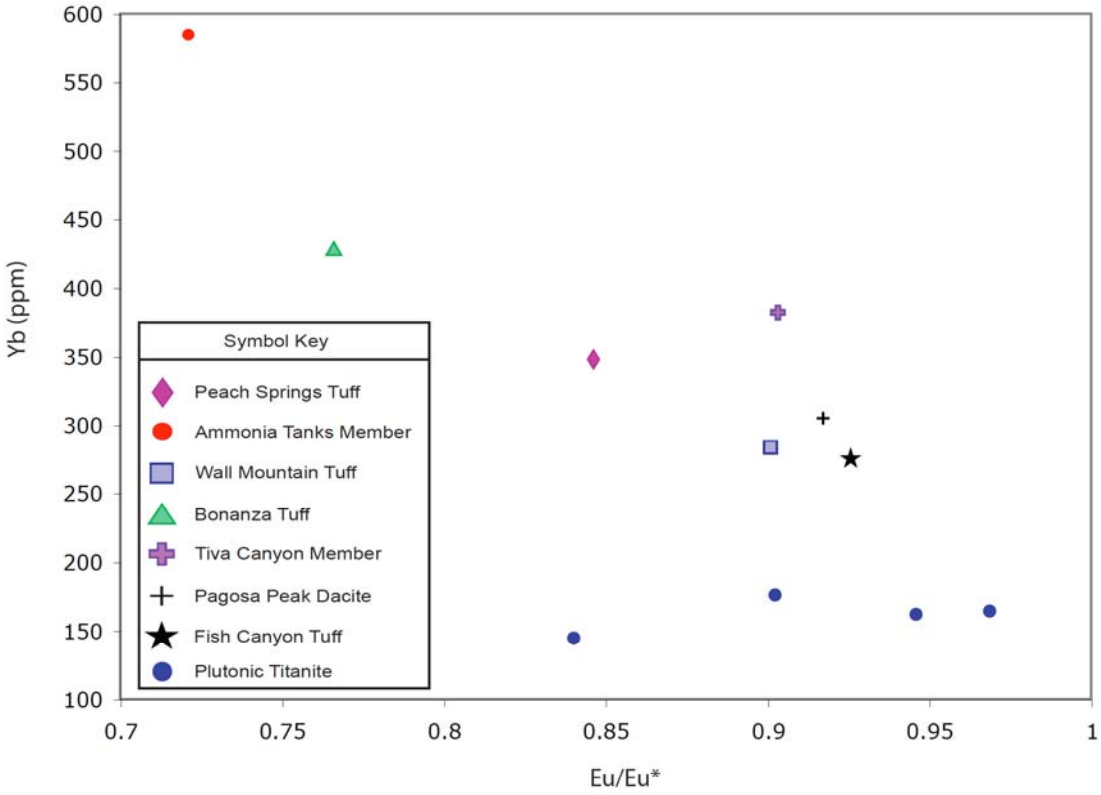

Figure 15: Eu/Eu* versus Yb concentration in titanite. Decreasing Eu/Eu* implies increased melt fractionation. This is due to the depletion of Eu in the melt by feldspar fractionation. Eu/Eu*of titanite would be expected to decrease with increased fractionation and incompatible element enrichment of the melt. This is supported by the negative correlation between Eu/Eu* and Yb concentration in volcanic titanites. While the Yb content of volcanic titanite increases with increasing melt fractionation, the Yb concentration of plutonic titanite remains relatively constant over a range of Eu/Eu* values.

where Sm_N, Gd_N and Eu_N are the chondrite-normalized values of titanite composition. Both titanite and groundmass from this study exhibit negative europium anomalies. Eu/Eu*of titanite is expected to decrease with increased fractionation and incompatible element enrichment of the melt. Figure 15 shows this trend, plotted as Eu/Eu* versus Yb concentration in titanite. In general, volcanic titanite crystals with larger negative Eu anomalies have higher concentrations of other REEs (in particular the HREEs), suggesting crystallization from a more fractionated melt. Conversely, there is no slope between Eu/Eu* and the REE content of plutonic titanite, despite differences in the formation of the Mount Princeton Batholith and Sierra Nevada Batholith titanite. This is likely due to the competition between titanite and other REE-bearing phases in plutonic rocks depleting the REEs in the melt phase. If plutonic titanite crystallized early from a high melt-fraction system as opposed to near-solidus conditions, a trend similar to that displayed by the volcanic titanite is expected.

V. CONCLUSIONS

Titanite is confirmed as an important mineral in the trace-element evolution of felsic igneous systems. The principal new observations to come from this study include:

(1) Titanite in dacitic and rhyolitic systems partitions the REEs and Y over a wide range (e.g., Ce titanite/groundmass ratios range from 180 in the Wall Mountain Tuff to 570 in the Ammonia Tanks). The range of partitioning values is controlled by lattice strain (with an ideal cation radius near Gd) and melt polymerization, and is likely influenced by the water content of the melt. REE partitioning values are in good agreement with previous studies in volcanic systems (Bachmann, 2005), but vary markedly from experimental studies of different melt compositions. Strontium, Rb, and Pb are generally incompatible in titanite compared to groundmass concentrations, whereas Sc, Th, and U are compatible.

(2) Volcanic and plutonic titanite crystals exhibit distinct differences in their trace-element content, zoning and substitution mechanisms indicating formation from different magmatic environments. Volcanic titanite forms through down-T crystallization of high melt-fraction systems whereas plutonic titanite forms at near- or sub-solidus conditions.

(3) Each volcanic rock unit studied has unique titanite/groundmass partitioning behavior, demonstrating the sensitivity of titanite trace-element partitioning to crystallization environment. Continued research on the thermodynamic stability of titanite, the link between plutonic and volcanic titanite crystals, and quantification of volatile contents in silicic

magmas will strengthen titanite-based research, and afford a better picture of the processes involved in creating batholiths and volcanic eruptions.

REFERENCES

Andersen DJ, Lindsley DH (1988) Internally consistent solution models for Fe-Mg-Mn-Ti oxides: Fe-Ti oxides. American Mineralogist 73: 714-726

Bachmann O, Dungan MA, Lipman PW (2002) The Fish Canyon magma body, San Juan volcanic field, Colorado: Rejuvenation and eruption of an upper crustal batholithic magma chamber. Journal of Petrology 43: 1469-1503

Bachmann O, Bergantz GW (2008) Rhyolites and their Source Mushes across Tectonic Settings. Journal of Petrology 49(12):2277-2285

Bachmann O, Dungan MA, Bussy F (2005) Insights into shallow magmatic processes in large silicic magma bodies: the trace element record in the Fish Canyon magma body, Colorado. Contributions to Mineralogy and Petrology 149:338-349

Bateman PC (1992) Plutonism in the central part of the Sierra Nevada Batholith, Calfornia. US Geological Survey, Professional Papers. 1483: 1-186

Bateman PC, Chappell BW (1979) Crystallization, fractionation, and solidification of the Tuolumne Intrusive Series, Yosemite national Park, California. Geological Society of America Bulletin 90(1):465-482

Bindeman IN, Schmitt AK, Valley, JW (2006) U-Pb zircon geochronology of silicic tuffs from the Timber Mountain/Oasis Valley caldera complex, Nevada: rapid generation of large volume magmas by shallow-level remelting. Contributions to Mineralogy and Petrology 152: 649-665

Belkin HE, De Vivo B, Lima A, Torok K (1996) Magmatic (silicates/saline/sulfur-rich/CO2) immiscibility and zirconium and rare-earth element enrichment from alkaline magma chamber margins: evidence from Ponza Island, Ponine Archipelago, Italy. European Journal of Mineralogy 8: 1401-20

Blundy J, Wood B (1994) Prediction of crystal-melt partition coefficients from elastic moduli. Nature 372:452-454

Brice JC (1975) Some thermodynamic aspects of the growth of strained crystals. Journal of Crystal Growth 28: 249-253

Browne B, Izbekov P, Eichelberger J, Churikova T (2010) Pre-eruptive storage conditions of the Holocene dacite erupted from Kizimen Volcano, Kamchatka. International Geology Review 52(1):95-110

Broxton DE, Warren RG, Byers FM, Scott RB (1989) Chemical and Mineralogic

Trends Within the Timber Mountain-Oasis Valley Caldera Complex, Nevada: Evidence for Multiple Cycles of Chemical Evolution in a Long-Lived Silicic Magma System. Journal of Geophysical Research 94(**B5**):5961-5985

Broska I, Harlov D, Tropper P, Siman P (2007) Formation of magmatic titanite and titanite-ilmenite phase relations during granite alteration in the Tribec Mountains, Western Carpathians, Slovakia. Lithos 95: 58-71

Byers FM Jr., Carr WJ, Orkild PP, Quinlivan WD, Sargent KA (1976) Volcanic suites and related cauldrons of Timber Mountain-Oasis Valley caldera comple, southern Nevada. United States Geological Survey Professional Paper 919; 1-70

Carmichael ISE, Nicholls J (1967) Iron-titanium oxides and oxygen fugacities in volcanic rocks. Journal of Geophysical Research 72: 4665-4687.

Carmichael ISE (1991) The redox states of basic and silicic magmas: a reflection of their source regions? Contributions to Mineralogy and Petrology 106:129-141

Chapin CE, Lowell GR (1979) Primary and secondary flow structures in ash-flow tuffs of the Gribbles Run paleovalley, central Colorado. In Chapin CE, Elston WE (eds) Ash-flow Tuffs. Geological Society of America Special Paper 180: 137-154

Cherniak DJ (1995) Sr and Nd diffusion in titanite. Chemical Geology 125:219-232

Christiansen RL, Lipman PW, Carr WJ, Byers FM Jr, Orkild PP, Sargent KA (1977) Timber Mountain-Oasis Valley caldera complex of southern Nevada. Geological Society of America Bulletin 88: 943-959

Davis JW (2010) Thermochronology and cooling histories of plutons: Implications for incremental pluton assembly. PhD Dissertation, University of North Carolina at Chapel Hill

Della Ventura G, Bellatreccia F, Williams CT (1999) Zr- and LREE-rich titanite from Tre Croci, Vico Volcanic complex (Latium, Italy). Mineralogical Magazine 63: 123-130

Dickinson FW (1996) Porphyroblasts of barium-zoned K-feldspar and quartz, Papoose Flat, Inyo Mountains, California; genesis and exploration implications. In: Coyner AR, Fahey PL (eds) Geology and ore deposits of the American Cordillera, Reno, NV, United States, Geological Society of Nevada, Reno: 909-924

Flood TP (1987) Cyclic evolution of a magmatic system: The Paintbrush Tuff, SW Nevada volcanic field. Dissertation, Michigan State University

Flood TP, Vogel TA, Schuraytz BC (1989) Chemical evolution of a magmatic system: The Paintbrush Tuff, Southwest Nevada Volcanic Field. Journal of Geophysical Research 94: 5943-5960

Foley EB (2010) Characteristics of modal layering in the Round Valley Peak Granodiorite, eastern Sierra Nevada, California. MS Thesis, University of North Carolina at Chapel Hill

Frost BR, Chamberlain KR, Schumacher JC (2000) Sphene (titanite): phase relations and role as a geochronometer. Chemical Geology 172:131-148

Gaschnig, AM (2005) Cause, timing, and significance f brittle deformation in Little Lakes Valley, eastern Siera Nevada, California. MS Thesis, University of North Carolina at Chapel Hill

Ghiorso MS, Sack RO (1991) Fe-Ti oxide geothermometry: thermodynamic formulation and the estimation of intensive variables in silicic magmas. Contributions to Mineralogy and Petrology 108:485-510

Giannetti B and Luhr JF (1983) The white trachytic tuff of Roccamonfina Volcano (Roman Region, Italy). Contributions to Mineralogy and Petrology 84: 235-252

Glazner AF (1988) Stratigraphy, structure, and potassic alteration of Miocene volcanic rocks in the Sleeping Beauty area, central Mojave Desert, California. Geological Society of America Bulletin 100:242-435

Glazner AF, Coleman DS, Bartley JM (2008) The tenuous connection between high-silica rhyolites and granodiorite plutons. Geology 36(2):183-186

Glazner AF, Nielson JE, Howard KA, Miller DM (1986) Correlation of the Peach Springs Tuff, a large-volume Miocene ignimbrite sheet in California and Arizona. Geology 14:840-843

Graham AL, Ringwood AE (1971) Lunar basalt genesis: The origin of the europium anomaly. Earth and Planetary Science Letters 13: 105-115

Green TH, Pearson NJ (1986) Rare-earth element partitioning between sphene and coexisting silicate liquid at high pressure and temperature. Chemical Geology 55:105-119

Gromet LP and Silver LT (1983) Rare earth element distributions amng minerals ina granodiorite and their petrogenetic implications. Geochimica et Cosmochimica Acta 47: 925-939

Hart SR, Davis KE (1978) Nickel partitioning between olivine and silicate melt. Earth and Planetary Science Letters 40: 203-219

Henderson P (1980) Rare Earth Element Partitioning Between Sphene, Apatite and Other Coexisting Minerals of the Kangerdlugssuaq Intrusion, E. Greenland. Contributions to Mineralogy and Petrology 72:81-85

Hildreth W (1979) The Bishop Tuff: Evidence for the origin of compositional zonation in silicic magma chambers. In: Chapin CE, Elston WE eds. Ash-Flow Tuffs, Geological Society of America Special Paper 180: 43-75

Hildreth W, Wilson CJN (2007) Compositional Zoning of the Bishop Tuff. Journal of Petrology 48(5):951-999

Irving AJ, Frey FA (1978) Distribution of trace elements between garnet megacrysts and host volcanic liquids of kimberlitic to rhyolitic composition. Geochimica et Cosmochimica Acta 42:771-787

Jaeger WL, Drake MJ (2000) Metal-silicate partitioning of Co, Ga, and W: Dependence on silicate melt composition. Geochimica et Cosmocimica Acta 64: 3887-3895

Johnson BR, Glazner AF (2010) Formation of K-feldspar megacrysts in granodioritic plutons by thermal cycling and late-stage textural coarsening. Contributions to Mineralogy and Petrology 159:599-619

Johnson MC, Rutherford, MJ (1989) Experimentally determined conditions in the Fish Canyon Tuff, Colorado, magma chamber. Journal of Petrology 30:711-737

Kratzmann DJ, Carey S, Scasso RA, Naranjo J-A (2010) Role of cryptic amphibole crystallization in magma differentiation at Hudson volcano, Southern Volcanic Zone, Chile. Contributions to Mineralogy and Petrology 159:237-264

Kress VC, Carmichael SE (1991) The compressibility of silicate liquids containing Fe2O3 and the effect of composition, temperature, oxygen fugacity and pressure on their redox states. Contributions to Mineralogy and Petrology 108: 82-92

Kretz R (1983) Symbols for rock-forming minerals. American Mineralogist 68: 277-279

Liferovich RP, Mitchell RH (2005) Composition and paragenesis of Na-, Nb- and Zr-bearing titanite from Khibina, Russia, and crystal-structure data for synthetic analogues. The Canadian Mineralogist 43:795-812

Lipman PW (1966) Water pressures during differentiation and crystallization of some ash-flow magmas from southern Nevada. American Journal of Science 264: 810-826

Lipman PW (1971) Iron-titanium oxide phenocrysts in compositionally zoned ash-flow sheets from southern Nevada. Journal of Geology 79:438-456

Lipman PW, Dungan M, Bachmann O (1997) Comagmatic granophyric granite in the Fish Canyon Tuff, Colorado: Implications for magma-chamber processes during a large ash-flow eruption. Geology 25: 915-918

Lipman PW (2007) Incremental assembly and prolonged consolidation of Cordilleran magma chambers: Evidence from the Southern Rocky Mountain volcanic field. Geosphere 3(1):42-70

Lipman PW and McIntosh WC (2008) Eruptive and noneruptive calderas, northeastern San Juan Mountains, Colorado: Where did the ignimbrites come from? Geological Society of America Bulletin 120: 771-795

Luhr JF, Carmichael ISE, Varekamp JC (1984) The 1982 eruptions of El Chichon volcano, Chiapas, Mexico: mineralogy and petrology of the anhydrite-bearing pumices. Journal of Volcanology and Geothermal Research 23:69-108

Mahood G, Hildreth W (1983) Large partition coefficients for trace elements in high-silica rhyolites. Geochimica et Cosmochimica Acta 47:11-30

Marks MAW, Coulson IM, Schilling J, Jacob DE, Schmitt AK, Markl G (2008) The effect of titanite and other HFSE-rich mineral (Ti-bearing andradite, zircon, eudialyte) fractionation on the geochemical evolution of silicate melts. Chemical Geology 257:153-172

Maughan LL, Christiansen EH, Best MG, Gromme CS, Deino AL, Tingey DG (2002) The Oligocene Lund Tuff, Great Basin, USA: a very large volume monotonous intermediate. Journal of Volcanology and Geothermal Research 113:129-157

McIntosh WC, Chapin CE (2004) Geochronology of the Central Colorado volcanic field, Colorado. In Cather SM, McIntosh WC, Kelley SS (eds) Tectonics, geochronology, and volcanism in the Southern Rocky Mountains and Rio Grande Rift. New Mexico Bureau of Geology, Bulletin 160: 205-238

McLeod GW, Dempster TJ, Faithfull JW (2011) Deciphering magma-mixing processes using zoned titanite from the Ross of Mull Granite, Scotland. Journal of Petrology 52: 55-82

Mills JG, Jr., Saltoun BW, Vogel TA (1997) Magma batches in the Timber Mountain magmatic system, Southwest Nevada Volcanic Field, Nevada, USA. Journal of Volcanology and Geothermal Research 78: 185-208

Mysen BO (1983) The structure of silicate melts. Annual Review of Earth and Planetary Sciences 11:75-97

Mysen BO (2004) Element partitioning between minerals and melt, melt composition, and melt structure. Chemical Geology 213:1-16

Nagasawa H, Schnetzler CC (1971) Partitioning of rare earth, alkali and alkaline earth elements between phenocrysts and acidic magma. Geochimica et Cosmochimica Acta 35: 953-968

Nakada S (1991) Magmatic processes in titanite-bearing dacites, central Andes of Chile and Bolivia. American Mineralogist 76:548-560

Nielson JE, Lux DR, Dalrymple GB, Glazner AF (1990) Age of the Peach Springs Tuff, Southeastern California and Western Arizona. Journal of Geophysical Research 95(B1):571-580

Noyes HJ, Frey FA, Wones DR (1983). A tale of two plutons: geochemical evidence bearing on the origin and differentiation of the Red Lake and Eagle Peak plutons, Central Sierra Nevada, California. Journal of Geology 91:487-509

Oberti R, Smith DC, Rossi G, Caucia F (1991) The crystal-chemistry of high-aluminium titanites. European Journal of Mineralogy 3:777-792

Olin PH (2010) Partitioning of rare earth and high field strength elements between titanite and phonolitic liquid. Poster session presented at: Geological Society

Pallister JS, Thornber CR, Cashman KV, Clynne MA, Lowers HA, Mandeville CW, Brownfield IK, Meeker GP (2008) Petrology of the 2004-2006 Mount St. Helens Lava Dome- Implications for Magmatic Plubing and Eruption Triggering. In: Sherrod DR, Scott WE, Stauffer PH (eds) A volcano Rekindled: The Renewed Eruption of Mount St. Helens, 2004-2008, vol U.S. Geological Survey Professional Paper 1750. pp 647-702

Pamukcu AS (2010) The evolution of the Peach Springs Tuff magmatic system as revealed by accessory mineral textures and compositions. MS Thesis, Vanderbilt University

Paterson BA, Stephens WE (1992) Kinetically induced compositional zoning in titanite: implications for accessory-phase/melt partitioning of trace elements. Contributions to Mineralogy and Petrology 109:373-385

Prowatke S, Klemme S (2005) Effect of melt composition on the partitioning of trace elements between titanite and silicate melt. Geochimica et Cosmochimica Acta 69(3):695-709

Prowatke S, Klemme S (2006) Rare earth element partitioning between titanite and silicate melts: Henry's law revisited. Geochimica et Cosmochimica Acta 70:4997-5012

Renne PR, Swisher CC, Deino AL, Karner DB, Owens TP, DePaolo DJ (1998) Intercalibration of standards, absolute ages and uncertainties in 40Ar/39Ar dating. Chemical Geology 145:117-152

Ribbe PH (1982) Titanite (sphene). In: Ribbe PH (ed) Orthosilicates, vol 5.

Shannon RD (1976) Revised effective ionic radii and systematic studies of interatomic distances in halides and chalcogenides. Acta Crystallographica A32:751-767

Shore M, Fowler AD (1996) Oscillatory zoning in minerals: a common phenomenon. The Canadian Mineralogist 34: 1111-1126

Simmons EC, Hedge CE (1978) Minor-element and Sr-isotope geochemistry of Tertiary stocks, Colorado mineral belt. Contributions to Mineralogy and Petrology 67: 379-396

Stimac J, Hickmott D, Abell R, Larocque ACL, Broxton D, Gardner J, Chipera S, Wolff J, Gauerke E (1996) Redistribution of Pb and other volatile trace metals during eruption, devitrification, and vapor-phase crystallization of the Bandelier Tuff, New Mexico. Journal of Volcanology and Geothermal Research 73:245-266

Stormer JC, Jr. (1983) The effects of recalculation on estimates of temperature and oxygen fugacity from analyses of multicomponent iron-titanium oxides. American Mineralogist 68:586-594

Sun SS, McDonough WF (1989) Chemical and isotopic systematics of oceanic basalts: implications for mantle composition and prcesses. In: Saunders AD, Nory MJ (eds) Magmatism in ocean basins. Geological Society [London] Special Publication 42: 313-345

Takahashi E (1978) Partitioning of Ni^{2+}, Co^{2+}, Fe^{2+}, Mn^{2+} and Mg^{2+} between olivine and silicate melts: compositional dependence of partition coefficient. Geochimica et Cosmochimica Acta 42: 1829-1844

Varga R, Smith B (1984) Evolution of the Early Oligocene Bonanza Caldera, northeast San Juan Volcanic Field, Colorado. Journal of Geophysical Research 89: 8679-8694

Venezky DY, Rutherford MJ (1997) Preeruption conditions and timing of dacite-andesite magma mixing in the 2.2 ka eruption at Mount Rainier. Journal of Geophysical Research 102(B9):20069-20086

Verhoogen J (1962) Distribution of titanium between silicates and oxides in igneous rocks. American Journal of Science 260:211-220

Vuorinen JH, Halenius U (2005) Nb-, Zr- and LREE-rich titanite from the Alno alkaline complex: Crystal chemistry and its importance as a petrogenetic indicator. Lithos 83:128-142

Watson EB (1976) Two-Liquid Partition Coefficients: Experimental Data and Geochemical Implications. Contributions to Mineralogy and Petrology 56:119-134

Watson EB (1977) Partitioning of manganese between forsterite and silicate liquid. Geochimica et Cosmochimica Acta 41:1363-1374

Watson EB, Liang Y (1995) A simple model for sector zoning in slowly grown crystals: Implications for growth rate and lattice diffusion, with emphasis on accessory minerals in crustal rocks. American Mineralogist 80:1179-1187

Whitney JA, Stormer JC, Jr. (1985) Mineralogy, Petrology and Magmatic Conditions from the Fish Canton Tuff, Central San Juan Volcanic Field, Colorado. Journal of Petrology 26(3):726-762

Winchester JA, Floyd PA (1977) Geochemical discrimination of different magma series and their differentiation products using immobile elements. Chemical Geology 20: 325-343

Wones DR (1989) Significance of the assemblage titanite + magnetite + quartz in granitic rocks. American Mineralogist 74:744-749

Xirouchakis D, Hirschman MM, Simpson JA (2001) The effect of titanium on the silica content and on mineral-liquid partitioning of mantle-equilibrated melts. Geochimica et Cosmochimica Acta 65:2201-2217

Xirouchakis D, Lindsley DH, Andersen DJ (2001a) Assemblages with titanite (CaTiOSiO4), Ca-Mg-Fe olivine and pyroxenes, Fe-Mg0Ti oxides, and quartz: Part I. Theory. American Mineralogist 86:247-253

Xirouchakis D, Lindsley DH, Frost BR (2001b) Assemblages with titanite (CaTiOSiO4), Ca-Mg-Fe olivine and pyroxenes, Fe-Mg-Ti oxides, and quartz: Part II. Application. American Mineralogist 86:254-264

Zhang L-S, Scharer U (1996) Inherited Pb components in magmatic titanite and their consequence for the interpretation of U-Pb ages. Earth and Planetary Science Letters 138:57-65

Zielinsky, RA (1982) The mobility of Uranium and other elements during the alteration of rhyolite ash to montmorillonite: A case study in the Troublesome Formation, Colorado, U.S.A. Chemical Geology 35: 185-204